Mechanistic study of dark etching regions in bearing steels due to rolling contact fatigue

Mostafa El Laithy[a], Ling Wang[a], Terry J. Harvey[a], Alexander Schwedt[b], Bernd Vierneusel[c], Joachim Mayer[b]

[a]*National Center for Advanced Tribology at Southampton (nCATS), University of Southampton, University Road, Southampton SO17 1BJ, UK*

[b]*Central Facility for Electron Microscopy (GFE), RWTH Aachen University, Ahornstraße 55, 52074 Aachen, Germany*

[c]*Schaeffler Technologies AG & Co. KG, Georg-Schäfer-Straße 30, 97421 Schweinfurt, Germany*

Abstract

Dark etching region (DER) formation is the first stage of a series of subsurface microstructural alterations induced by cyclic stresses during rolling contact fatigue in bearing steels followed by the formation of low angle bands (LAB) and high angle bands (HAB). A unified formation mechanism for LAB and HAB development in bearing steels has been proposed as a series of energy build-up and release in a recent study. This paper presents the development of DER through the analysis of two different steel, 100Cr6 and 50CrMo4, at various stages in the lifetime of bearings using SEM, EBSD and nanoindentation. It is found that early stages of DER consist of patches of multiple dark etching bands orientated at four distinct orientations relative to the rolling direction. As the dark etching bands grow in density, they contribute to the refinement of the parent microstructure through fragmentation of martensite laths. The fragmentation as well as intersections of dark etching bands lead to the creation of stress points within the region that become nucleation sites for the formation of equiaxed ferrite grains through recrystallization, which has been found to be the initiation stage of LAB. Hence this study establishes a link between DER and LAB/HAB development in rolling bearings.

1. Introduction

Rolling element bearings are essential components in rotating machinery for industries ranging from automotive and aerospace to naval and power transmission. As a result, there is a continuous drive towards extending bearing life and enhancing their performance. The cyclic stresses induced on rolling element bearings during rolling contact fatigue (RCF) have been observed to result in the formation of subsurface microstructural alterations known as dark etching regions (DERs) and white etching bands (WEBs) [1]. The investigation of these features is considered essential to develop a detailed understanding of the material response of bearing steels during RCF

to improve the performance of bearings and develop more detailed RCF prediction model on late stage bearing durability. For the sake of clarity and to emphasize the differences between the studies: DER and WEBs are generally believed to be different from other microstructural alterations such as butterflies and white etching cracks (WECs). The latter typically develops in the early life of bearings under 'special harmful conditions' and can be considered detrimental [2, 3, 4].

DER and WEB have been known for several decades [5, 1, 6, 7, 8] and their designations were given based on their etched appearance under light optical microscopy (LOM), where DERs refers to a microstructural alteration that appears to be dark whereas WEB have a white appearance due to their high resistance to etchants [9, 1, 10, 11]. DERs has been reported to form from approximately 5 million stress cycles but can be heavily influenced by both the contact pressure and operating temperature of bearings, and typically DERs forms earlier under higher contact pressure and operating temperature [12, 7, 1, 13].

The overall DERs are seen as a sickle shape in bearing inner ring subsurface when observed in axial cross-sections (perpendicular to rolling direction) and as a band parallel to the raceway surface in circumferential cross-sections (parallel to the rolling direction) with a depth varying between 100 and 650 μm from the surface depending on contact pressure and bearing geometry [7, 11, 12, 14, 6]. The width of DER band in circumferential direction and the density of dark patches increases with increasing stress cycles [10]. While it is generally accepted that DER formation is a consequence of martensite decay due to stress induced phase transformation [12, 15], its formation mechanism, e.g. the process of martensite decay, is still contested. It has been reported that the DER consists of a ferrite phase with inhomogenously distributed excess carbon and remains of the parent microstructure (typically martensite [12]), however the driving mechanisms for the transformation between the two phases is under debate. One of the earliest theories by Bush et al. [6] reported that DERs develop in the region of the maximum orthogonal shear stress and resembles tempered martensite. This theory suggested that the DER formation process initiates when martensite crystallites within the vicinity of yielding carbides, causing dislocation pile-ups at martensite/carbide interfaces through an intrusion/extrusion mechanism. Given that DERs are also reported to only develop at contact pressures above 2.5 GPa (i.e. beyond the shakedown limit of the material), it was suggested that plastic deformation plays a major role in the microstructural transformation. Swahn et al. [12] however suggested that DER formation is linked to the redistribution of carbon from within the martensite lattice to dislocations, leading to an accumulation of plastic deformation. This was confirmed by TEM images of DERs containing 'transformed zones' and 'residual martensite' during the early stage and only 'transformed zones' at the late stage. However, no further investigation was conducted to analyse the transformed zones to identify the

details. Voskamp [11] proposed a stress induced phase transformation theory, suggesting that cyclic stresses in the subsurface can cause a local temperature increase and encourage diffusion of atomic carbon within the martensite matrix. As a consequence, dislocations that were previously pinned by carbon are 'unpinned', leading to the activation of potential slip systems through plastic deformation.

The most recent investigation by Fu et. al [9] proposed a strain-induced carbon migration mechanism, guided by dislocation gliding driven by the orthogonal stress component of the Hertzian contact pressure. The theory suggests that the build-up of strain due to cyclic stresses unpins dislocations from carbon Cottrell atmospheres, and dislocation gliding then re-attracting free carbon leading to a carbon flux till the carbon atoms reach the vicinity of nano-sized tempered carbides. The model is based on thickening of tempered carbides through dislocation assisted carbon-migration. However, it is discovered that the time for carbon to segregate at dislocations according to the dislocation-assisted carbon migration theory is orders of magnitude larger than the overrolling frequency at which the bearings were operating i.e. the duration between two adjacent stress applying moments on a certain area [16]. However, there have been conflicting reports on which stress component is responsible for the DER formation. Other reports have correlated the DER with the principal shear stress [7, 17], von Mises [18] and residual stresses [19]. While another study has proposed the positioning of the DER in the subsurface changes with cycles as it becomes consumed by newly formed WEBs [10]. Hence a systematic investigation of the DER position in the subsurface from early to late stages is needed to clarify this.

Nonetheless a prominent feature that has been neglected in the above proposed formation mechanisms is the so called 'elongated structure', which have been given different names in experimental studies including ferrite microbands [20], deformation bands [6], dark needles [21], persistent slip bands [8] and elongated ferrite grains [16, 22]. It thus remains unclear what these features really are and their involvements in the DER formation process. Smelova et al. [22] demonstrated that DERs contain both elongated ferrite grains and equiaxed ferrite grains formed through dynamic recrystallization. They identified the equiaxed grains formation due to their low misorientation in the DER compared to that in the unaltered matrix as well as the existence of high angle grain boundaries between grains and gamma-fibre texture. It has also been reported that 'slip marks' or 'elongated grains' in DER are orthogonal to each other and are at an angle of 45° to the bearing surface in another study [23]. This contradicts the findings from an earlier study by Sugino et al. [24], who suggested that newly formed dark etching patches/bands were directionally oriented towards undamaged martensite platelets. Other orientations have also been reported in literature for dark etching patches/bands [12, 25]. It is thus necessary to investigate and clarify the inclinations of elongated structures in DER [22].

The hardness of DER is another area of debate in literature. Some found an increase of up to 100 HV in DERs comparing with that of the parent martensitic structure and suggested it due to work hardening of the martensite matrix or the transformation of retained austenite to martensite [5, 21], while others recorded a reduction of up to 150 HV and suggested it due to carbon migration and ferrite formation [26, 9, 12, 6, 1]. Most of these studies have used a micro-hardness indenter for the analysis of the DER hardness, this means the interaction will likely much bigger than some individual microstructure features, leading to different findings in literature.

While a link between the formation of LAB and HAB is established as a form of repetitive cycle of energy build-up and release within steel microstructures [27], no publication has shown a direct link between DERs and the initiation of LABs. This study aims to investigate the formation mechanism and evolution of DERs and clarify their hardness through the analysis of early and late-stage DERs. Two bearing steels, including a standard bearing steel 100Cr6 and a lower carbon steel 50CrMo4 have been investigated to study DER formation under two carbon content levels over a range of stress cycles using light optical microscopy (LOM), Scanning electron microscopy (SEM), electron backscatter diffraction (EBSD) and nanoindentation techniques. An additional aim is to establish a link between the development of DERs and the initiation of LABs.

2. Methodology

Inner rings of RCF tested angular contact ball bearing (ACBBs) 7205 B made from two steels (martensitic 100Cr6 and 50CrMo4), are cut into samples for the investigation in this study. The 100Cr6 bearing steel was tempered at 230°C for 2 hours while the 50CrMo4 sample was tempered at 160°C for 2 hours. Analysis is conducted on both cross-sections in the axial (perpendicular to rolling direction) and circumferential (parallel to rolling direction) cuts.. The compositions of the steel alloys used in this study were obtained using spark emission spectroscopy and are shown in Table 1.

Table 1 Chemical Compositions of the bearing steels.

Material:	Wt%											
	C	Si	Mn	P	S	Cr	Ni	Mo	Cu	V	Al	O
100Cr6	0.93	0.3	0.34	0.01	0.004	1.49	0.02	0.005	0.066	0.004	0.002	0.0012
50CrMo4	0.44	0.24	0.66	0.008	0.001	1.17	0.75	0.25	0.12	0.087	0.024	-

2.1 RCF Testing

ACBBs of the two steels that have been RCF tested on L-17 bearing life test rig at Schaeffler Technologies [28] under a wide range of conditions to create DER and WEBs at different formation stages. All bearing tests have

been conducted under a maximum contact pressure of 2.9 GPa and 12,000 rpm rotating speed over a range of pre-determined stress cycles (see details in Table 2) to investigate the DER formed at different stages. No surface damage is observed on any of the bearings analysed here. An ISO VG 68 lubricant was used and the bearing outer ring temperature was maintained at 80°C. The RCF tests were conducted under elastohydrodynamic lubrication conditions with a viscosity ratio κ of 2.69 (ratio of operating viscosity to reference viscosity).

2.2 Microstructural Characterization

The analysis of the microstructure of the bearing samples was conducted through standard metallographic preparation which includes cutting of bearing inner rings in both axial and circumferential cross-sections, mounting the cut specimens in Bakelite, followed by successive grades of mechanical grinding using SiC paper of 800, 1200 and 4000 grit then successive polishing using 3 µm, 1 µm and 0.25 µm diamond suspensions. The polished surfaces are later etched with 2% Nital to highlight microstructural features of interest formed in the samples. Etched samples are examined by an Olympus BX51 optical microscope and a JEOL JSM-6500F SEM with an accelerating voltage of 15 kV for secondary electron (SE) imaging. In section 3.3, Backscatter electron (BSE) imaging is performed after repolishing the sample surface with colloidal silica suspension (OP-S) using a GeminiSEM 300 by Carl Zeiss Microscopy. Selected samples are further analyzed through EBSD examination using a JEOL JSM-7000F SEM (equipped a EDAX Pegasus EBSD system) for grain structure analysis. Then a similar process of polishing and etching is performed as discussed previously to capture SE imaging for comparison. All EBSD evaluations have been performed with OIM analysis 8.0 by Ametek-EDAX. All IPF maps in this study shows the crystal axis parallel to the overrolling normal direction. Non martensite-martensite high angle grain boundary (non Ms-Ms HAGB) maps are derived by detecting all HAGB larger than 15°, then erase the grain boundary segments showing an axis/angle pair than lies within 5° tolerance close to the axis/angle pairs expected for the classical orientations found in martensite (Kurdyumov-Sachs, Greninger-Troiano, Nishiyama-Wassermann and Pitsch [29] [30] [31] [32]). In KAM maps, the notation (100 nm, 5°) is used to refer the the canalysis condition where the average grain orientation change of up to 5° of the crystal lattice is measured over a distance of 100 nm. For all EBSD analysis, an accelerating voltage of 15 kV and probe current of approximately 30 nA have been used with a step size of 50 nm.

Nano-indentation was performed on selected samples using a NanoTest Vantage (Micro Materials Ltd.) system with a Berkovich tip to examine the hardness distribution in subsurface of the bearing inner rings relevant to DER development. Samples are polished with colloidal silica suspension (OP-S) to obtain a deformation-free surface

with minimal surface roughness in accordance with BS EN ISO 14577-1:2015 standards. The maximum penetration depth for the indentation map was set to 900 nm with a fixed loading/unloading rate of 10 mN/s. All tests include a 10 s dwell time at the maximum load and thermal drift correction data is enabled with a collection time of 60 s.

Table 2 A summary of the ACBBs investigated in this study

Material	Contact Pressure (GPa)	Stress Cycles for Inner Ring (Million)
100Cr6	2.9	0*
		591
		1116
		1690
		2342
		3016
50CrMo4	2.9	0*
		104
		158
		846
		1626
		2038
		7668

*This is a virgin bearing.

3. Results

3.1 DER Evolution Overview

DER formed in 100Cr6 at different stress cycles are shown in the optical images of the axial cuts of the bearings in Figure 1. It can be seen that, from small to large stress cycles (Figure 1a to e), the DER appearing in sickle shape grows slightly, however it is seen to be influenced by the growth of a bright region above the sickle due to formation of WEB [10, 27]. Additionally, the boundary of the DER is not very sharp, i.e. the changes between the DER and the parent microstructure below and the bright region above are gradual/diffuse. Within the shallower WEB region in Figure 1d) and e), HAB can be differentiated from LAB in the axial cross section as the later

appears as thin bands while the former appears as large white ‘blocks’ in the order of 100-200 µm.

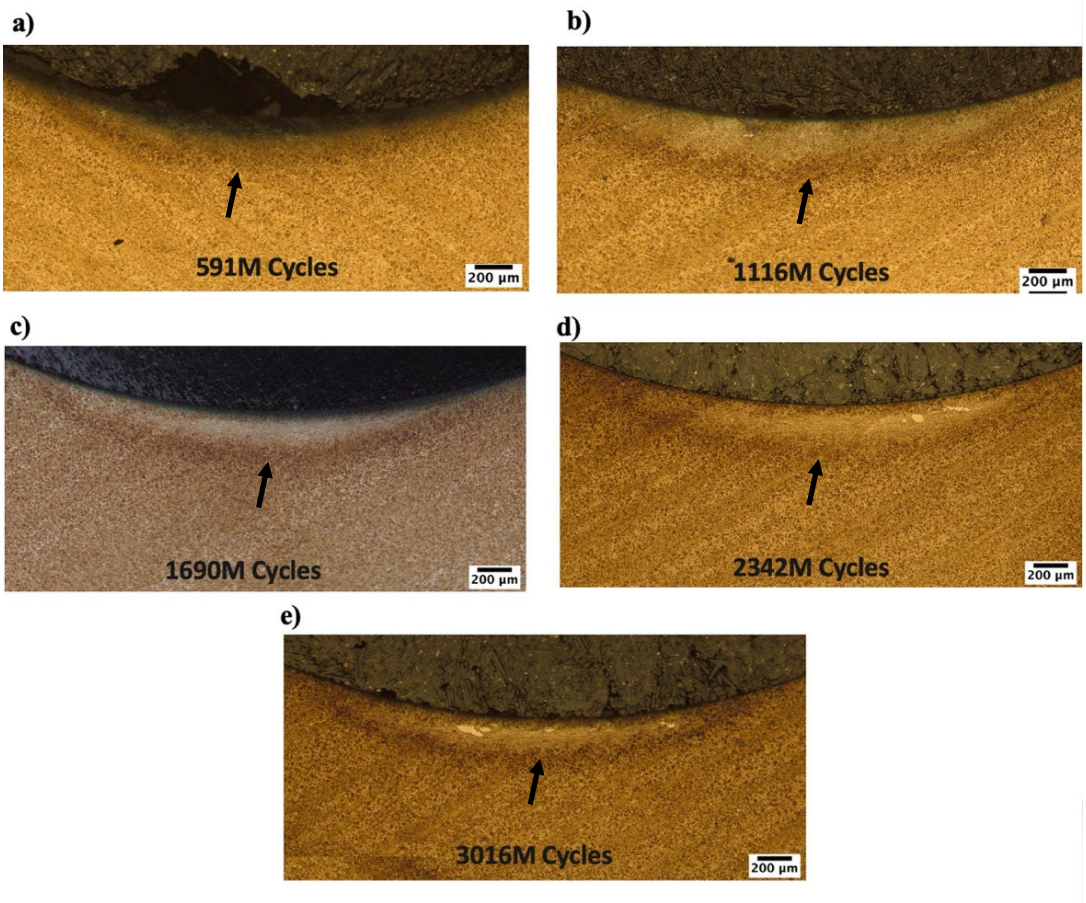

Figure 1: Axial cross section of 100Cr6 martensite samples showing the sickle shape DER in samples run for a) 591, b) 1116, c) 1690, d) 2342 and e) 3016 million cycles. Black arrows indicate the middle of the sickle shape DER.

LOM images of the DER formed in the 50CrMo4 bearings (in axial cuts) are shown in Figure 2. Interestingly no obvious sickle shape of DER is observed in the early stages (as shown in the samples in a-b), but rather a crescent shape where the DER grow very close to the contacting surface. The density and area of the DER also appears to increase with stress cycles. At later stages (seen from sample 2c onwards), a sickle shape start to appear similar to that in 100Cr6 (see Figure 1), however the top part of the dark patch is gradually replaced by brighter regions. This is observed along with the delayed development of WEBs in 50CrMo4 compared to the 100Cr6 samples [33], suggesting that DER development in the 50CrMo4 is much more gradual than that in 100Cr6. Also, DER in the early stages (Figure 2a-d) has a more distinct boundary comparing with those in later stages in a sickle shape

showing diffuse boundaries (Figure 2e-f), similar to that observed in the 100Cr6 samples.

The position of the upper and lower boundaries as well as the center of the DER and WEBs in the bearing subsurface at the middle of the contact from Figure 2 is plotted in Figure 3 in comparison to the subsurface stress distribution, similar to the approach taken in [10]. The DER formed in the subsurface of 100Cr6 bearings do not correlate with the corresponding subsurface stress distribution as previously reported in [10], possibly due to the rapid formation of WEBs masking the true DER thus affected the analysis on DER. With the much slower DER development observed in 50CrMo4, the early stage DER (crescent shape) seem to be correlated with the orthogonal shear stress distribution (Figure 3), similar to that reported in [6, 34]. Like the DER in 100Cr6, the

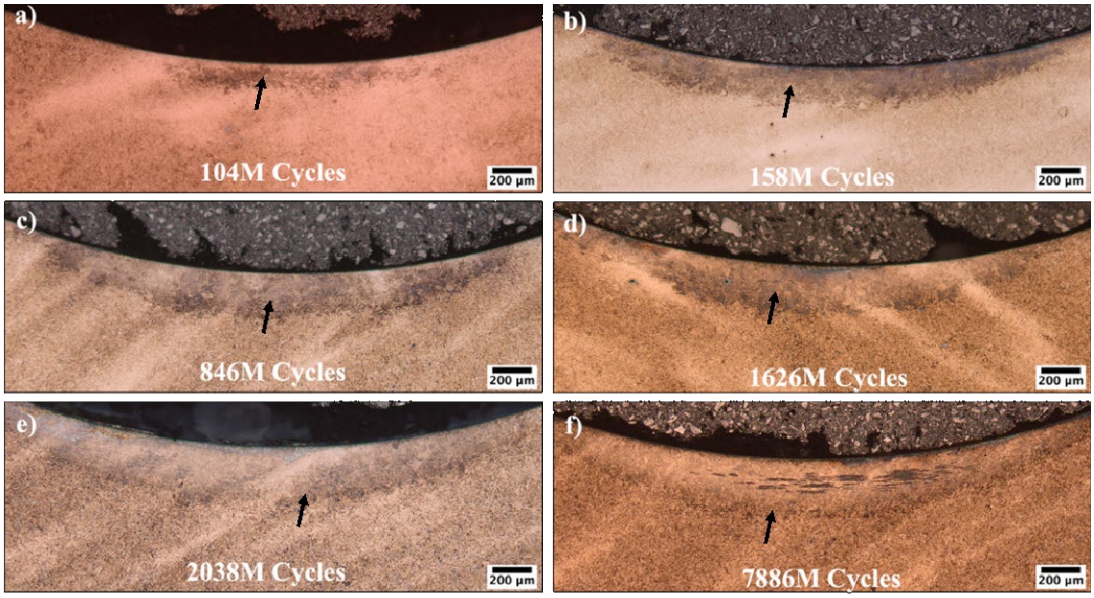

Figure 2: LOM images of the axial cross section of 50CrMo4 bearings showing the DER in samples run under 2.9 GPa for a) 104, b) 158, c) 846, d) 1626, e) 2038 and f) 7668 million cycles. Black arrows is used to indicate the middle of the DER.

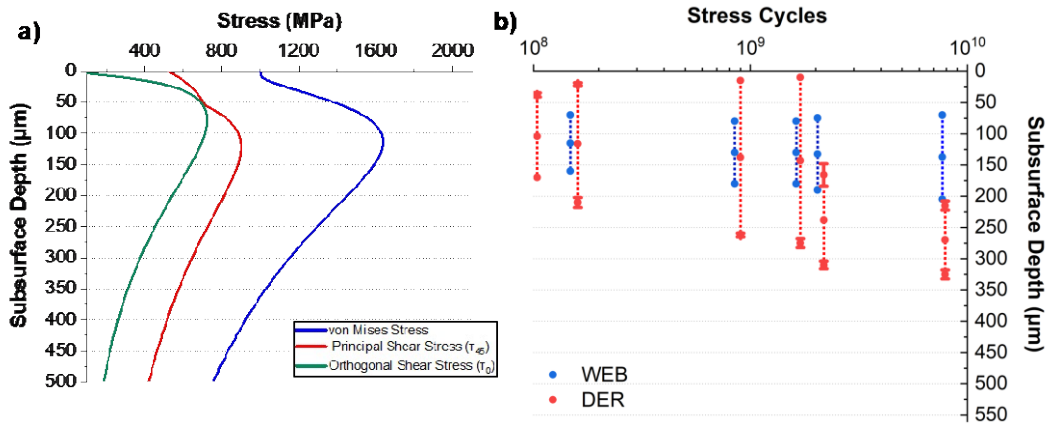

Figure 3: Depths of DER and WEBs formed in the 50CrMo4 test samples vs the corresponding subsurface stresses. a) Distributions of the subsurface stresses, including von Mises stress σ_{vM}, principal shear stress τ_{45} and orthogonal shear stress τ_0. b) Positions of the DER and WEBs in subsurface, showing their upper and lower boundaries and the middle points in each of the tested samples.

sickle shaped DER in 50CrMo4 (later stages) also does not correlate with the corresponding stresses due to the development of 'brightened' area in the top part of the DER. Again, similar to that in the 100Cr6, the 'brightened' area above the DER sickle in 50CrMo4 bearings (same area where WEB develops in the 100Cr6 samples) correlates well with the maximum von Mises stresses (Figure 3). This suggests that at a later stage of DER development, a 'brightening' process starts in the DER at the maximum von Mises stress region leading to the formation of LAB (see them in Figure 2e&f in the axial cut and Figures 4e&f in circumferential cuts appearing as a dark band). The brightening of the DER and development of LABs in the DER in 50CrMo4 bearings are clearly observed in Figure 4 of the circumferential cross-sections. The dark appearance of the LABs in Figure 2f and in Figure 4e&f are the result of using polarized light to enhance the contrast and highlighting the DER more clearly.

As 50CrMo4 produced DER formation at a much slower rate, than 100Cr6, it will be explored first and then a comparison will be made between the two steels .

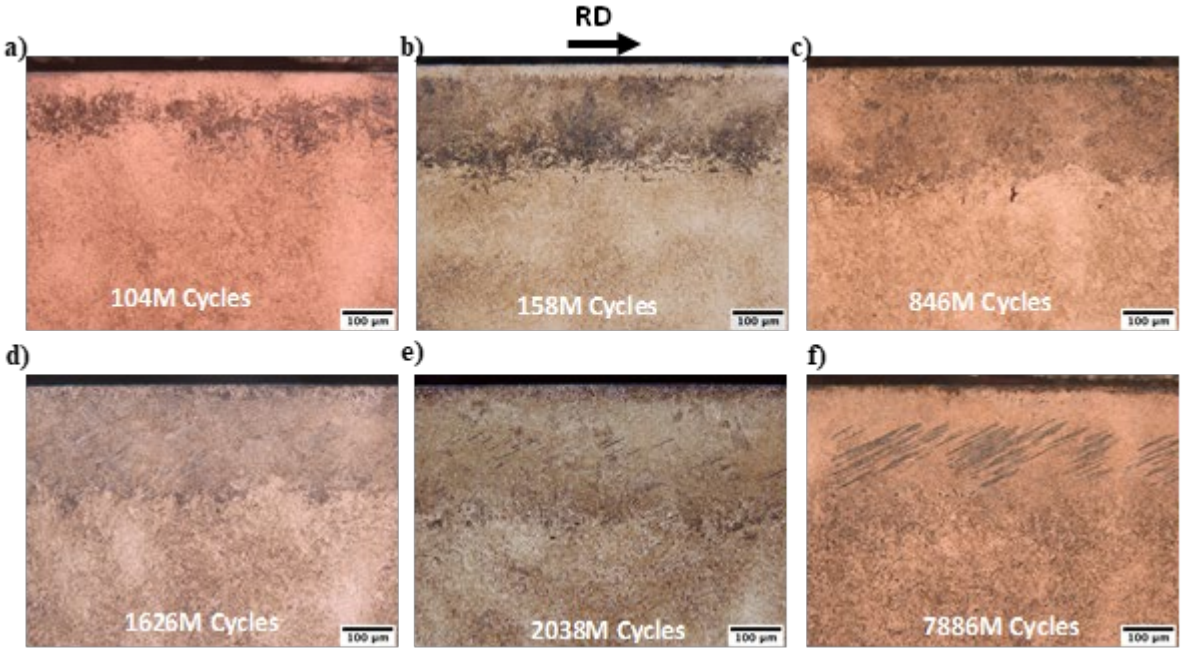

Figure 4: LOM images of DER and LAB in circumferential cross section of 50CrMo4 martensite samples run under 2.9 GPa for a) 104 b) 158 c) 846 d) 1626 e) 2038 and f) 7668 million stress cycles.

3.2 DER in 50CrMo4 Bearing Steel

Figure 5 presents various SEM images of a virgin bearing sample of martensitic 50CrMo4, showing typical martensitic features such as martensite laths and a homogeneous strain distribution in the IQ map (Figure 5c) with no obvious texturing being detected (Figure 5b) as expected. It however does

not show to have spherical primary carbides that is a distinctive difference from the 100Cr6 steel due to the lower carbon content in 50CrMo4.

Figure 6 shows the DER in the 50CrMo4 bearing after 104 million cycles, where they appear as patches in the LOM and are shown to consist of heavily etched dark etching bands in the SE SEM images. The dark etching bands in Figure 6b-e have an estimated width ranging from 30 to 100 nm and length reaching up to 7 µm.

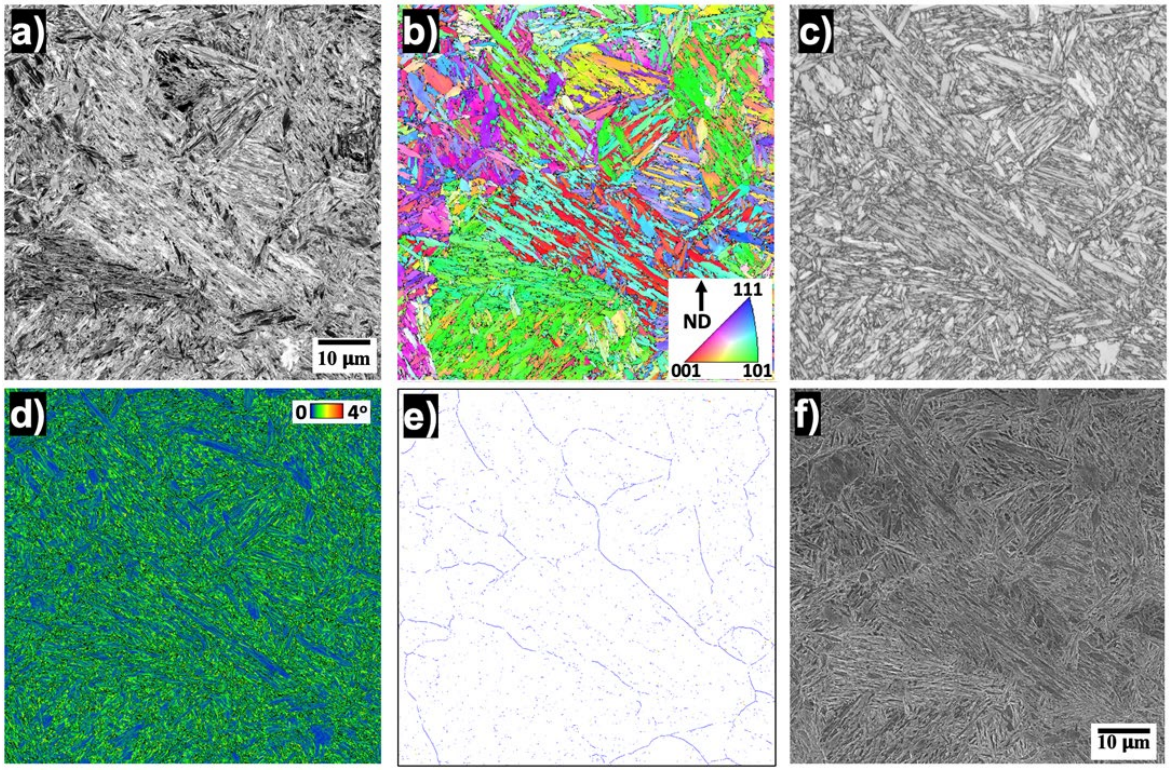

Figure 5: SEM images showing the microstructures of a virgin 50CrMo4 bearing. a) BSE SEM image b) IPF Map (crystal axis parallel to ND) c) IQ Map d) KAM Map (100 nm, 5◦) e) Non-martensite-martensite HAGB map and f) SE SEM image of the area in Nital-etched condition.

A close look of the DER in a 104 million cycles sample has shown that the dark etching areas relate to the bands (Figure 6). It is also noticed that adjacent to the dark etching bands, some bright or white structures are seen, (yellow arrows in Figure 6b-e), which are thought to be a form of carbides due to their high resistance to etching, which is similar to that of the lenticular carbides in WEBs [27]. However, it is challenging to confirm their composition due to their extremely small sizes.

To investigate the orientations of these dark etching bands with respect to the rolling direction, stitched images of high-resolution SEM images covering an area of 130 x 180 µm of the DER has been

captured from the sample run for 158 million cycles as shown in Figure 7b. Thresholding of the SEM image has been applied using ImageJ (see example in Figure 7a) to distinguish the bands from the surrounding microstructure. Data filters have been applied to remove noise and only capture features resembling the dimensions of the dark etching bands from SEM observations (aspect ratio > 3, thickness < 150 nm and circularity < 0.15). Overall, a total of approximately 2800 data points are captured. Applying this technique on the overall DER area (red area in Figure 7b), has shown the bands have preferential orientations of approximately 10-30°, 65-85° and 135-170°. It is interesting to note that the 10-30° is the most observed orientation (similar to LAB orientation) followed by the 65-75° orientation (similar to HAB orientations) as shown in Figure 7c. These two group orientations also have a sharper peak compared to the third orientation group shown in Figure 7c at 135-170°. To further investigate these orientations, different areas of the DER have been compared in the depth range where WEBs would develop (based on Figure 3 and [10, 33]). The Upper DER area shown in Figure 7b and Figure 7d interestingly shows the same three orientations groups being dominant but evenly distributed (this corresponds to the subsurface depth range where HAB would be expected to form [33]). In the deeper region labelled as lower DER in Figure 7b and Figure 7e, it is interesting that the overwhelming majority of bands lie within the first orientation group corresponding to that of the LAB. This statistical distribution orientation of the dark etching bands provide strong evidence linking the sequential development of DER, LAB and HAB. Furthermore, the different angle groups are often observed to overlap in dense dark etching band regions where individual bands become inseparable. At the junctions where two groups of different orientation bands interact, small equiaxed grains are seen to form (see areas highlighted by dashed yellow lines in Figure 7g), which is the next stage of DER evolution. Within the same image, thin nano-sized bright structures parallel to the dark etching bands are also observed, which are believed to be carbide structures as a result of carbon migration from the ferritic dark etching bands to their edges nucleating carbides based on their resistance to etching.

During the analysis of DER, it was noticed that the dark etching regions are not completely dark, i.e. is not composed of fully packed dark etching bands. It also contains 'bright patches', which appears to grow bigger and bigger within the DER during later stages. Detailed analysis of these 'bright' areas has shown that they consist of a finer grain structures (Figure 8b) compared to the dark etching bands (Figure 8c) and those in the original martensite (Figure 8d, taken from an area that 700 µm from the contacting surface in the same bearing, i.e. far away from the altered region). These fine grains are nano-size equiaxed grains resistant to the etchant, hence appear to be 'bright' in the structure. Bright nano-grains appear to start to form in dense dark etching band areas and as more and more nano-grains form, the dark etching band groups observed in earlier stages (see in Figures 6&7) become less and less visible. Eventually, the microstructure in the original DER consisting of dark etching

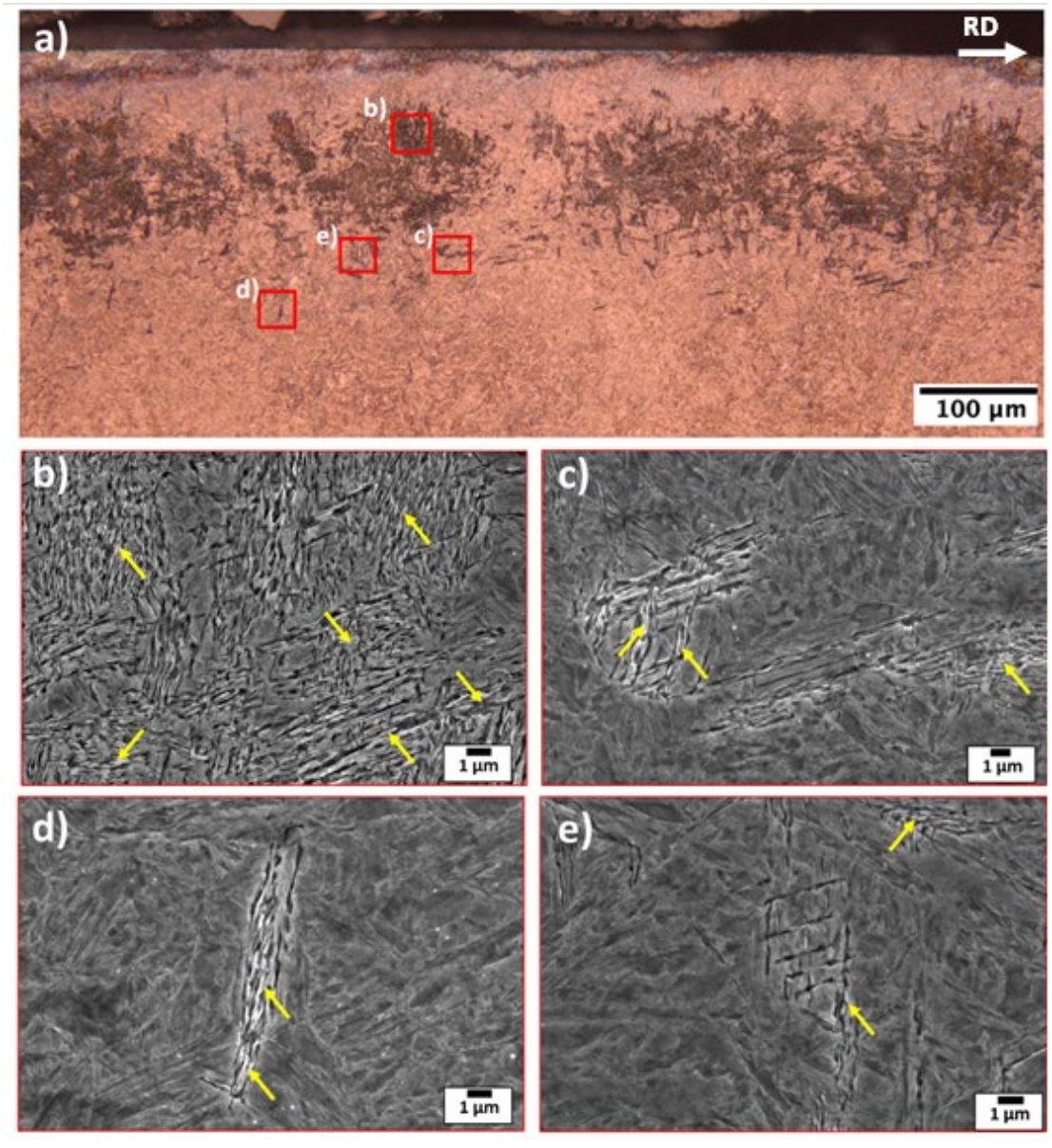

Figure 6: a) An optical image of DER in a 50CrMo4 sample run for 104 million cycles under 2.9 GPa. b-e) SEM images of areas indicated in a), showing dark patches of bands at multiple orientations in the DER.

bands is replaced by bright fine grains. It is thus proposed that the grain refinement process of a microstructural transformation has caused the brightening of the DER observed. The refined microstructure, as well as the carbides formed adjacent to the dark etching bands discussed earlier, may be responsible for the enhanced resistance to

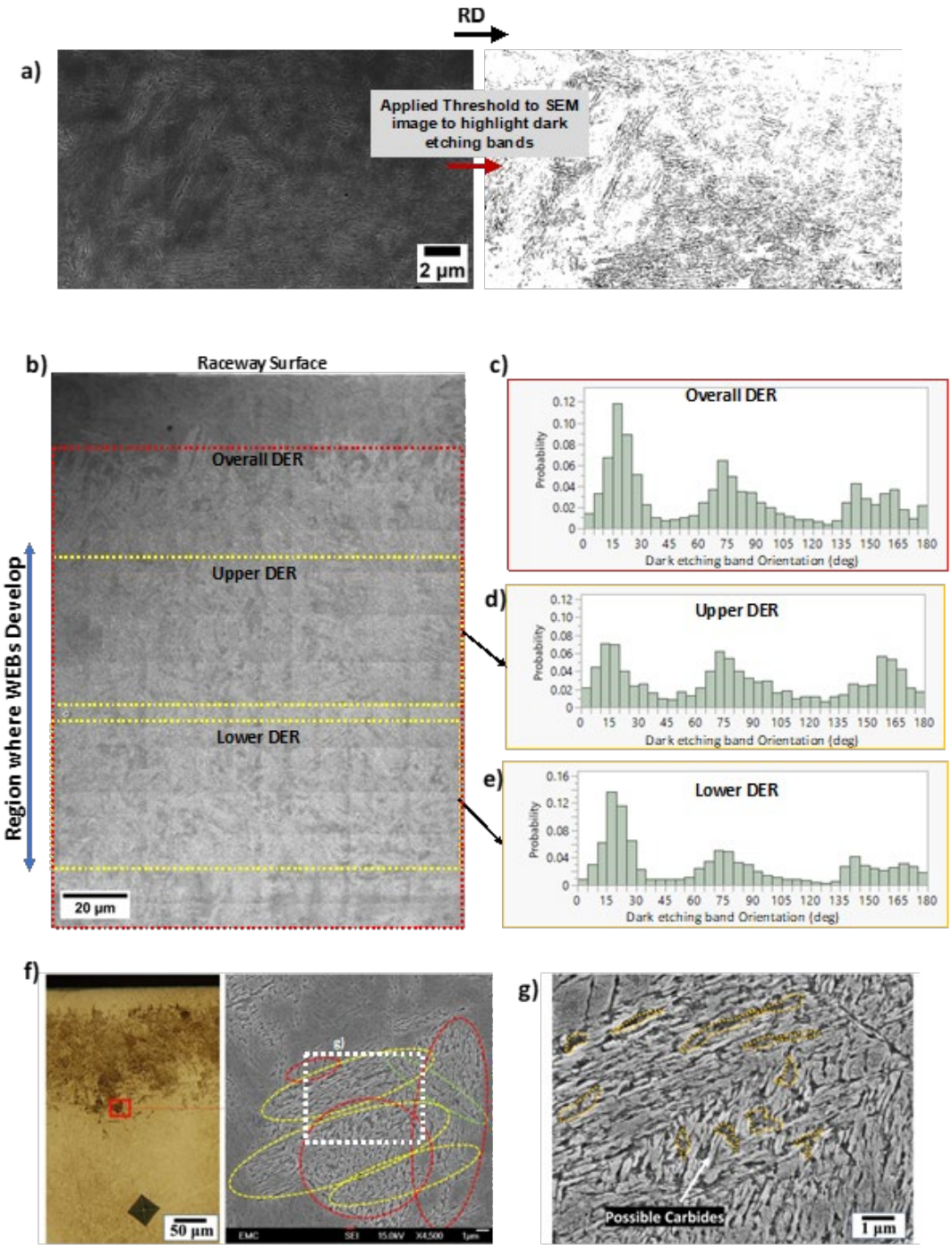

Figure 7: a) Illustration of thresholding technique used on SEM images of DER to distinguish the individual bands for orientation analysis. b) SEM image of subsurface covering the span of the DER. The probability distribution of the dark etching band orientation is measured across c) the overall DER based on red area in b), d) upper DER area highlighted in yellow in b) and e) lower DER area highlighted in yellow in b). f) Shows an optical and SEM image of a dark patch within the DER where different band orientation groups are highlighted in ellipses. g) High magnification of area highlighted in white in f) showing equiaxed grains formed within the dense dark etching band area and possible carbides forming parallel to the bands. Images taken from 50CrMo4 sample run for 158 million cycles.

etching as shown in Figure 4e,f.

To

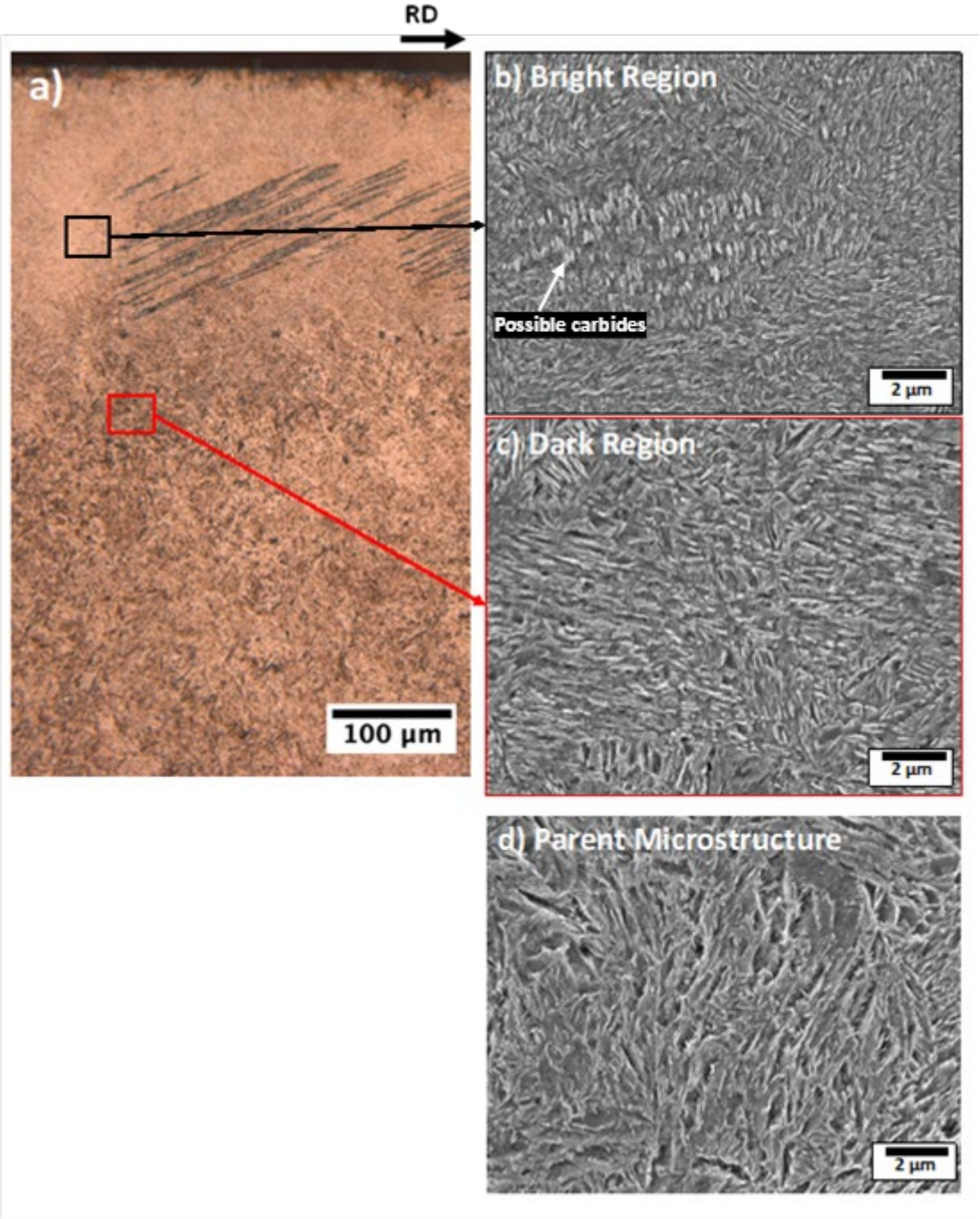

Figure 8: a) An Optical image from a 50CrMo4 bearing sample tested under 2.9 GPa for 7668 million cycles, showing both DER and LAB. b) An SEM image of an area from a), showing a bright part within the DER. c) An SEM image of an area from a), showing a dark part within the DER. d) An SEM image showing the parent microstructure (obtained from the same sample at 700 µm depth from the surface, i.e away from the maximum stress region.

summarize, DER initially appears as thin dark etching bands that grow in patches at four distinctive groups of orientations, resulting in the dark etching appearance under optical microscopy. The dark etching bands are observed to be accompanied by etch-resistant structures at their edges, which are believed to be carbides formed

from the carbon migrating from the dark etching ferrite bands. Later the ferrite bands break down due to formation of nano-grains through a refinement of the microstructure, leading to 'brightening' of the DER under LOM.

3.2 Comparison with 100Cr6 Bearing Steel

Not all the DER formation stages observed in 50CrMo4 have been seen in the 100Cr6 bearing samples due to lack of early stage samples (minimum stress cycle tested was 591 million cycles), the rapid development of DER and formation of WEB within the same regions [10, 33]. Overall, much less dark etching bands are formed in the 100Cr6 bearings than that in the 50CrMo4 bearings especially at low stress cycles. The dark etching bands in the 591 million cycles 100Cr6 bearing (Figure 9) are similar to that observed in the 104 million cycle 50CrMo4 bearing (Figure 6b-e) but are less dense and more dispersed, also supported by the difference in their dark etch responses shown in Figures 1 and 2. The dark etching bands formed in 100Cr6 samples have similar dimensions (< 100 nm width and < 7 μm length) and orientations to those in 50CrMo4 as presented in Figure 7. Similar to 50CrMo4, dense closely-packed dark etching bands parallel to each other (Figure 9f), equiaxed grains at intersections between dark etching bands of different orientations (Figure 9d and 9b) and bright carbide structures parallel to DER bands (Figure 9d & f) are observed in DER in 100Cr6.

At a much later stage in 100Cr6 after 3016 million stress cycles, WEB networks are seen to have fully developed and DER features are only visible in between individual LAB (Figure 10). The carbide structures developed parallel to the dark etching bands appear thicker and more pronounced in this sample comparing with those in the 50CrMo4 samples (etch resistant areas in Figure 7g vs Figure 10b), possibly due to the much higher carbon content in 100Cr6 alloy (Table 1). The measured thickness of the carbide structures highlighted in Figure 10b have a thickness of 520 ± 204 nm, while those in the 50CrMo4 sample (Figure 7g) show a thickness of 167 ± 42 nm. While this could be considered an artefact of the higher stress cycles (3016 million vs 158 million in Figure 10b and Figure 7b respectively), the white particles in Figure 8b resembling carbides also show an average thickness of 233 ± 53 nm (50CrMo4 sample run for 7886 million cycles). Considering that the microstructure of 50CrMo4 shows no primary carbides in contrast to 100Cr6, possible dissolution of primary or tempered carbides during RCF [35], which may lead to higher carbon contents in the martensite matrix in 100Cr6 compared to 50CrMo4, can contribute to enhanced thickening of the DER carbide structures in 100Cr6 samples compared to 50CrMo4. Again, the etching behavior of these carbide structures is observed to be similar to that of the lenticular carbides in LABs (discussed in [27]). This suggests a similar carbide formation mechanism in DERs as that in LABs [27]. Similar to that in the 50CrMo4, equiaxed grains are seen to have developed in regions with dense close-packed

DER bands and at intersections of DER bands at different orientations (Figure 10b).

The grain refinement observed in the 50CrMo4 during the late stages of the DER (Figure 8) has also been seen in 100Cr6 bearings (see in Figure 10 comparing features in the 591 and 3016 million cycles). The dark and bright contrast in the SEM images in Figure 10b and Figure 10d are correlated to refined grains and carbides due to their higher etchant resistance, suggesting DER bands breakdown and grain refinement occurring during the latest stage of DER development similar to DER development in 50CrMo4

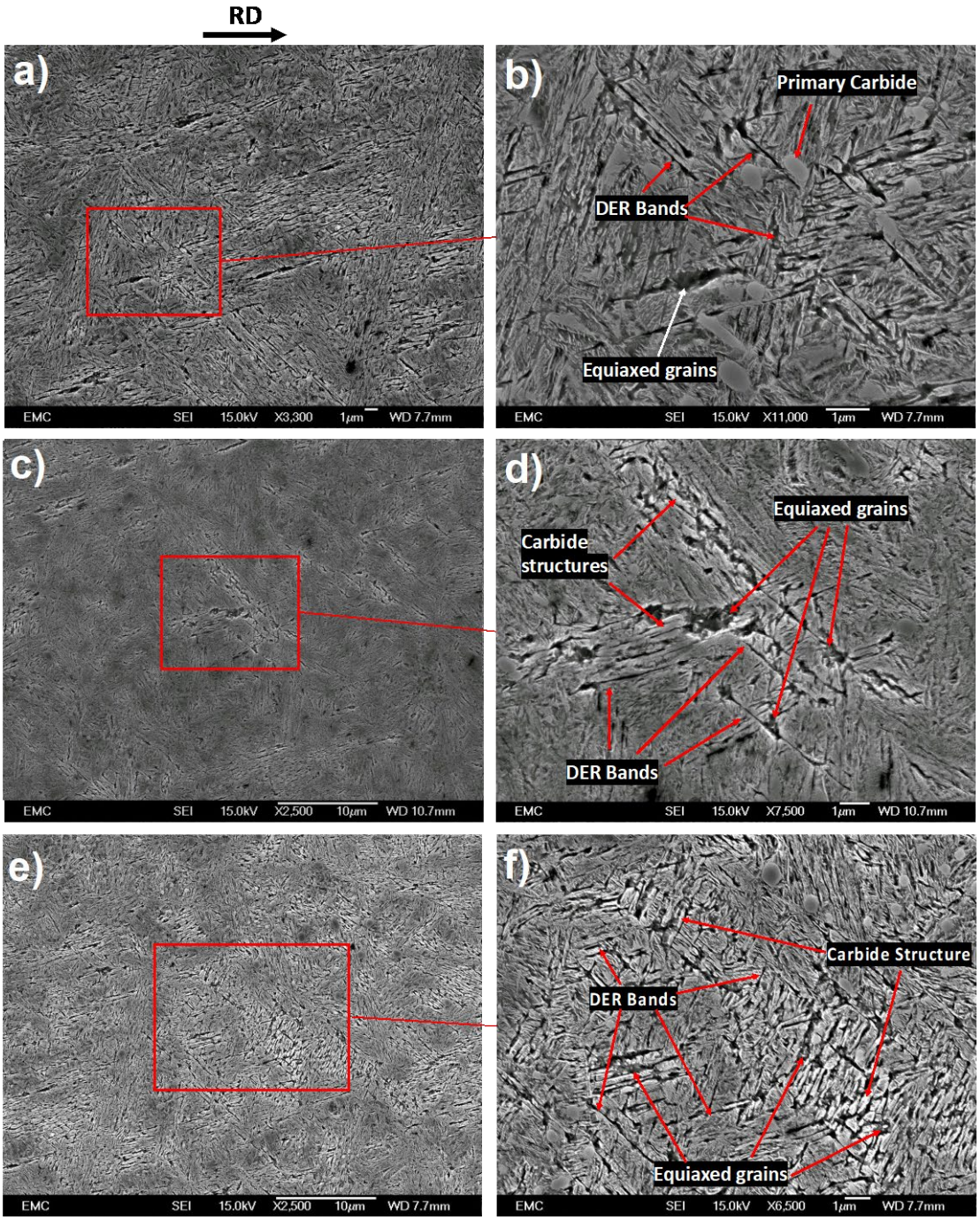

Figure 9: a,c,e) SEM images of DER areas within 100Cr6 sample run under 2.9 GPa for 591 million cycles at a depth below the lower boundary of LAB. b,d,f) High magnification images from a), c) and e) respectively showing individual DER bands, equiaxed grains and carbide structures.

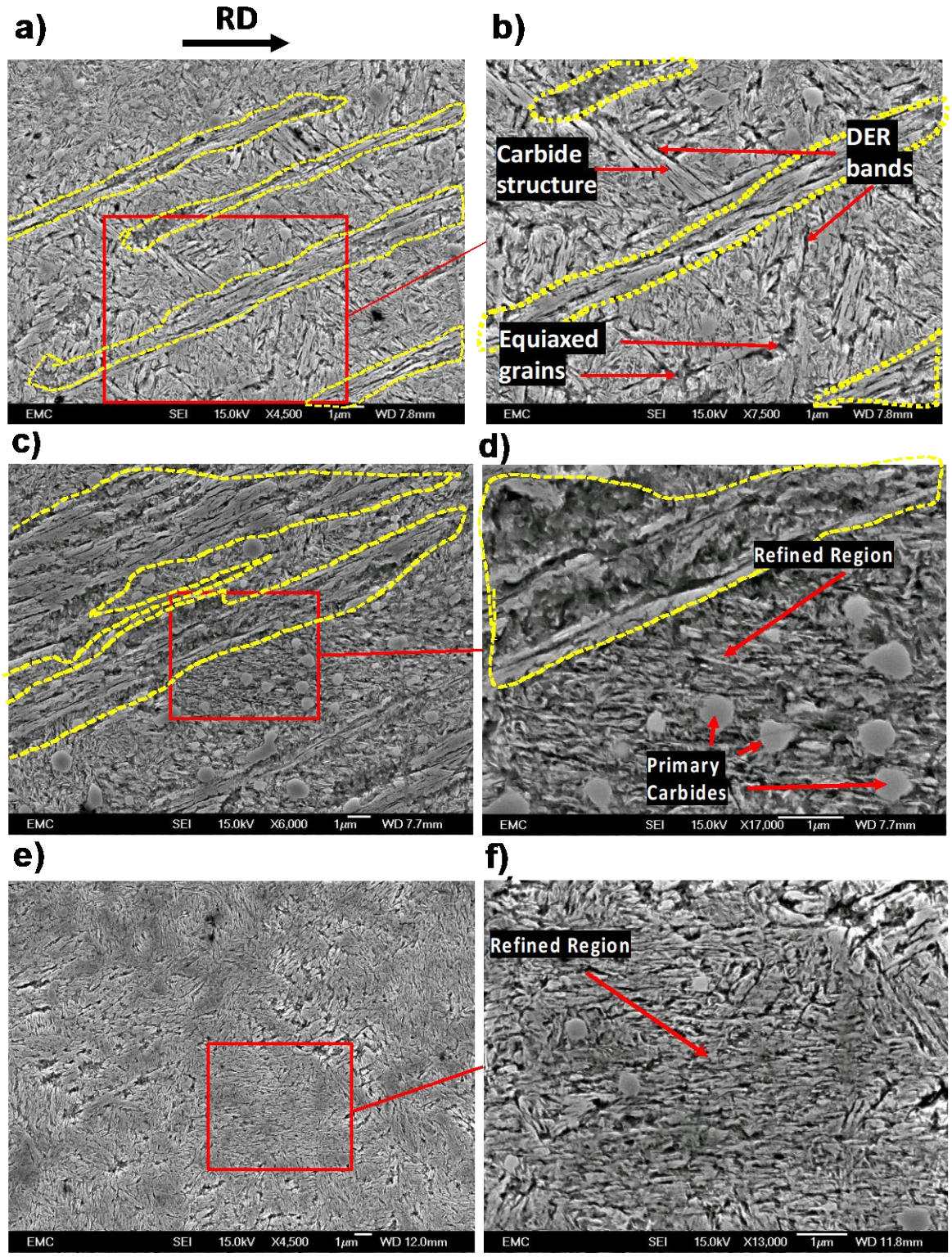

Figure 10: SEM images of DER features observed between LABs in a number of 100Cr6 samples, showing DER bands, equiaxed grains and carbide structures in a&b), and refined microstructure between LABs where DER bands become less pronounced in c,d,e and f). Images a-d) are from samples tested for 3016 million cycles and e&f) for 591 million cycles. . LAB features are highlighted in yellow.

3.3 EBSD analysis of DERs

To further investigate the assumptions made in the previous sections, including the formation dark etching bands at the early stage and the 'brightening' of the DER due to grain refinement at the late stage of DER formation in 50CrMo4, EBSD analysis was conducted on an early, medium and late stage sample with 104, 158 and 7886 million stress cycles respectively, these correspond to Figures 11, 12 and 13 respectively.

Figure 11 (early stage) shows individual dark etching bands (pointed by black arrows) causing fragmentation of a martensite lath which would contribute to the overall microstructure refinement discussed in the previous section. Given the dimension of these bands at this stage, it is difficult to fully analyse the structure of these bands. However, the KAM map and IQ maps shown in Figure 11c and 11e suggest greater defects at the edge of these bands, suggesting they are induced via plastic deformation and likely a form of deformation band. The area highlighted in Figure 11a seems to consist of dense closely-packed parallel bands and a much more refined grain structure can be seen in the equivalent EBSD maps in Figure 11b-e of this area. This suggests a refinement of the microstructure is due to various bands (closely packed) fragmenting the original martensite laths as shown at the black arrows in Figure 11. Further inspection of this refined area (shown in Figure 11c) indicates that this area consists of both low misorientation equiaxed grains (likely a product of recrystallization) and high misorientation fine grains (likely due to the refinement of the martensite due to dense dark etching bands). A gradual transition occurs within the DER, involving development of dense dark etching bands, leads to the refinement of the parent martensite and creation of high stress points within the microstructure which become nucleation sites for the recrystallization of equiaxed ferrite grains that have been observed in both DERs [22] and WEBs [27]. The refined region of the DER also presents no obvious texture (Figure 11b) while the non Ms-Ms HAGB map in Figure 11d suggests the formation of new grains in the refined region (recrystallization). Hence the dark etching bands transforms the microstructure through both 1) breakdown of parent martensite into finer grains and 2) causing recrystallization initiation sites due to high stress point accumulation.

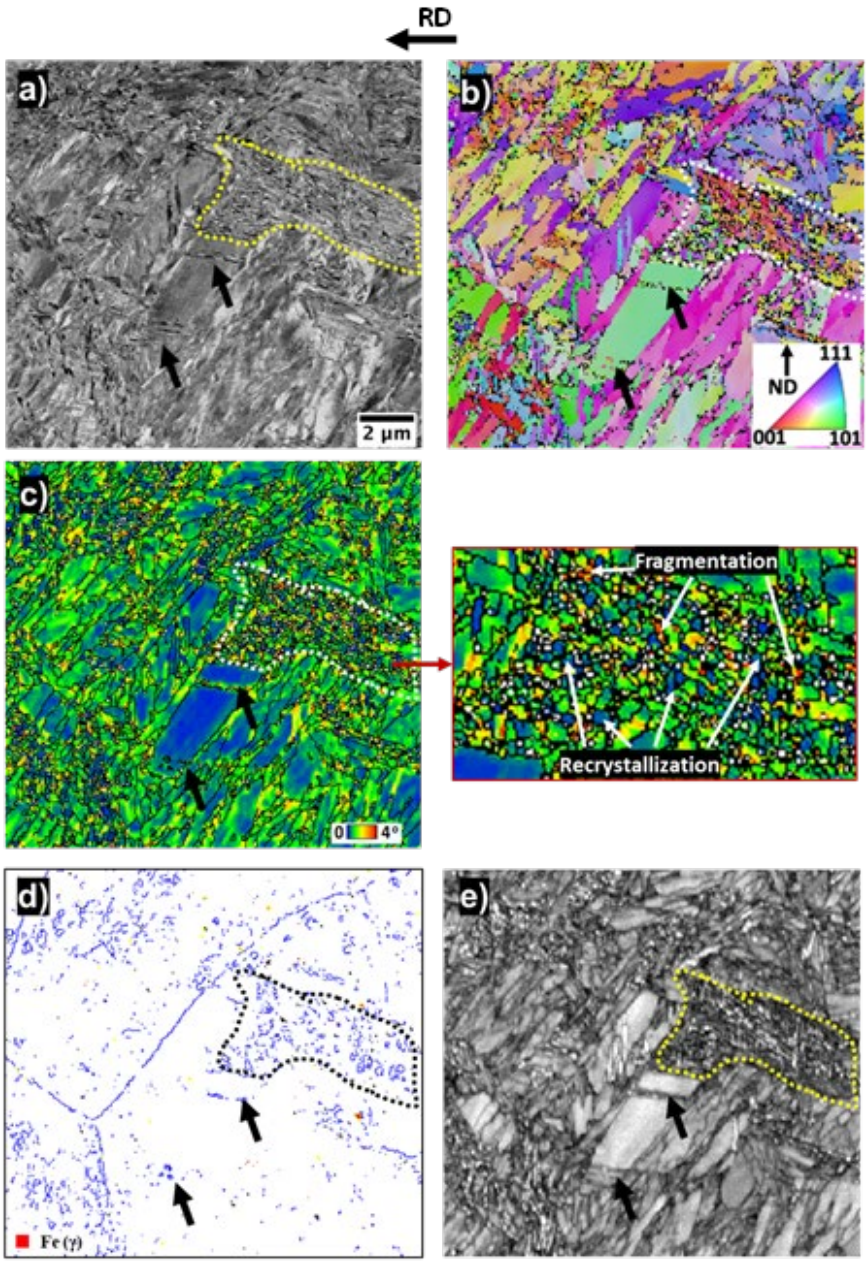

Figure 11: Analysis of DER in 50CrMo4 sample run under 2.9 GPa for 104 million cycles showing a) BSE SEM image b) IPF map (crystal axis parallel to ND) c) KAM Map (100 nm, 5°) d) non-martensite-martensite HAGB map and e) IQ map of DER bands causing martensite fragmentation (arrow) and highlighted region of dense DER bands consisting of refined grains. Image taken at a depth of 120 µm from surface.

The evolution of the DER is further investigated by analysing it at medium to late stage in samples run at 158 million and 7886 million respectively. For consistency, DER formed at similar stress levels, i.e. at the depth of 120 µm from the surface are compared. Comparing the DER features at this depth with those in Figure 4b and 4f, those in the 158 million sample and in the 7886 million cycle sample are equivalent to the 'dark' and 'bright' features respectively. The DER areas captured in Figure 12 surround individual LAB which are highlighted in red. The area highlighted in yellow between LABs in Figure 12, i.e. remaining DER, shows a clear overall refinement (Figure 12b,f) compared to the virgin material (Figure 5), and the refinement intensifies from the

medium (Figure 12a-d) to the late stage (Figure 12e-h) . However no clear texture development in the DER at both stages is observed from the IPF maps (Figures 12b and f). The etched SE SEM images at the two stages show that more dark etching bands are contained in the earlier stage (Figure 12c) than that in the later stage (Figure 12g), which explains the difference in etching response shown previously in Figure 4. More details of the area highlighted in yellow in Figure 12 can be seen in Figure 13 at a higher magnification.

A comparison between Figure 13c and 13g shows that the development of DER from medium to late stage involves the 'removal' of the dark etching bands (reduction of the number of bands from Figure 13c to g). The corresponding IPF maps in Figure 13b and f also show the continuous refinement experienced by the DER microstructure during the transition. This is a similar stage as that shown in Figure 11, where multiple dark etching bands breakdown the parent matrix into finer grains and multiple bands intersect contributing to the breakdown and leading to the final structure shown in Figure 13e-f. This breakdown of dark etching bands and refinement of parent matrix, the KAM maps show that the number of high stress points have also increased from the earlier stage (Figure 13d) to the later one (Figure 13h). This suggests that the increase in stress points in the microstructure correlates well with the refinement of the parent martensite. Low misorientation equiaxed grains can also be seen in Figure 13h, indicating that the stress points induced through the fragmentation process become nucleation sites for recrystallization as a form of energy release in the microstructure [27]. Bright fine structures adjacent to the dark etching bands observed in Figure 13c are suggested to be carbide structures due to their etching response and smooth appearance as previously suggested. Similar structures are also observed at the late DER stage shown in Figure 13g.

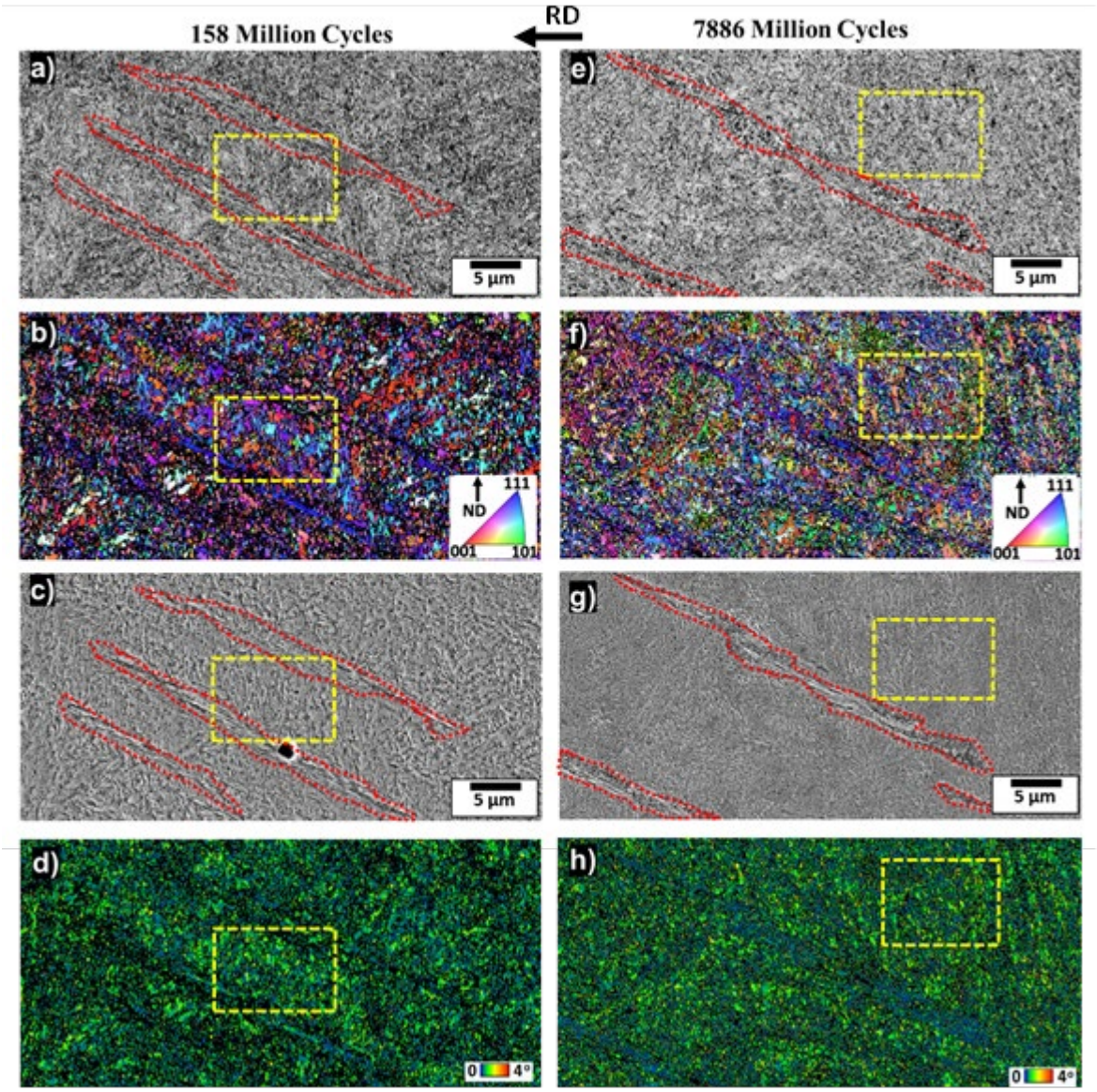

Figure 12: a) and c) BSE and SE SEM images of DER surrounding LAB in 50CrMo4 samples run for 158 million cycles while b) shows IPF map (crystal axis parallel to normal direction) and d) shows KAM map (100 nm, 5°) of area in a) and c). e) and f) BSE and SE SEM images of DER surrounding LAB in 50CrMo4 samples run for 7886 million cycles while f) shows IPF map (parallel to normal direction) and h) shows KAM map Map (100 nm, 5°) of area in e) and f). Images are captured at a depth of 120 µm from the surface.

EBSD analysis of a 100Cr6 sample (shown in Figure 14) shows that, refinement is observed in regions with dense dark etching bands where no obvious texture is shown (Figure 14b), a lower IQ contrast in the DER area (Figure 14e), suggesting more defects than the parent microstructure. The complete transformation of the region is evidenced in the HAGB map (Figure 14d), comparing with the non-transformed region in the upper left corner of images in Figure 14. The KAM map in Figure 14c also shows a build-up or high stress points (high misorientation) in the DER region (as indicated by the arrows in the figure) surrounded by the low misorientation equiaxed grains which is a typical product of recrystallization. The etch-resistant features can also be seen adjacent to the dark etching bands in Figure 14f. This is similar to the findings in Figure 11 and hence confirms similarities in the

formation mechanism of DERs in both steels.

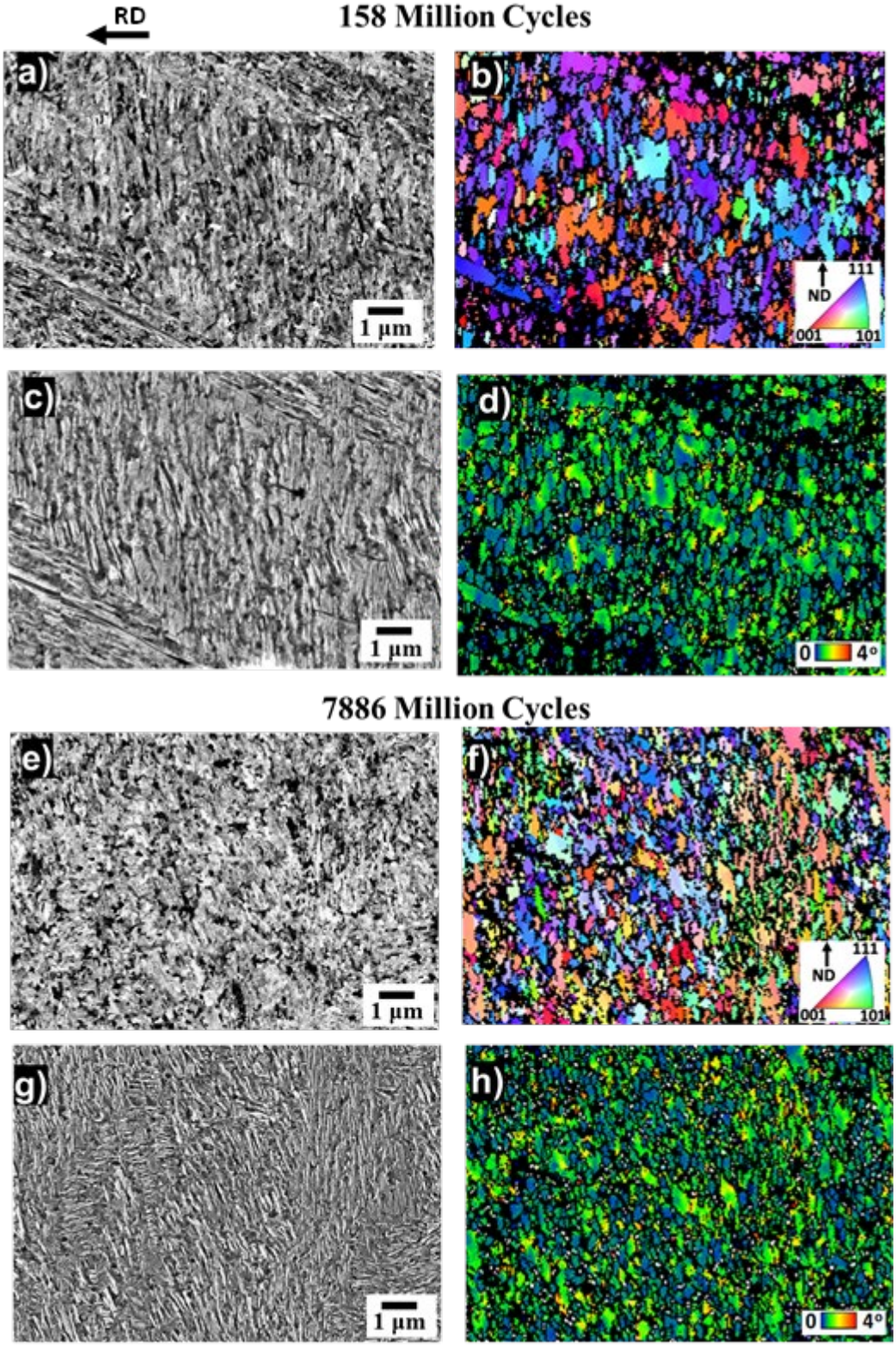

Figure 13: Enlarged images of highlighted regions in Figure 12 showing a,e) BSE SEM images, b,f) IPF map (crystal axis parallel to normal direction (ND)), c,g) SE SEM image and d,h) KAM map (100 nm, 5°). a-d) corresponds to sample run for 158 million cycles while e-h) corresponds to sample run for 7886 million cycles.

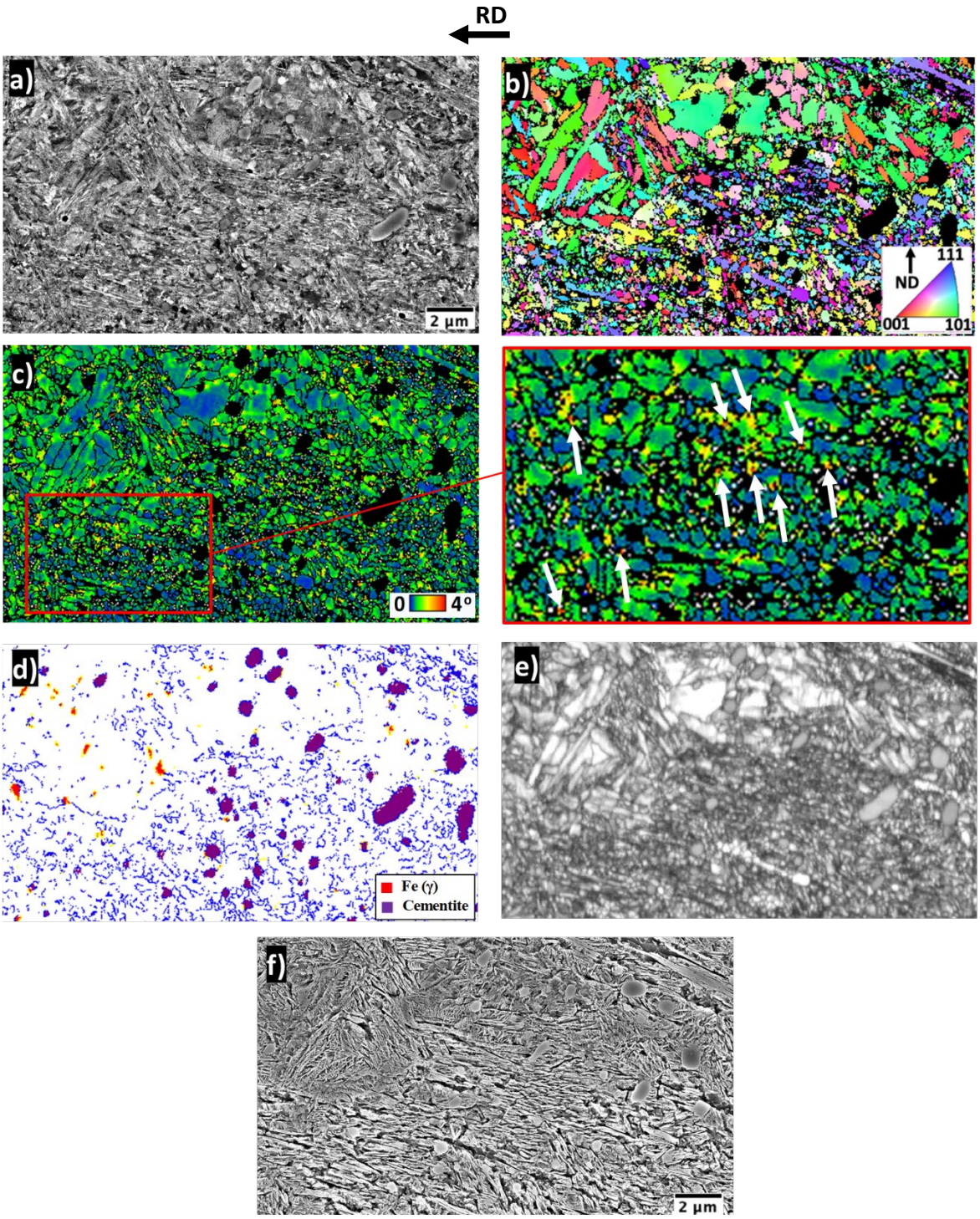

Figure 14: Analysis of DER in 100Cr6 sample run for 591 million cycles showing a) BSE SEM image b) IPF map (crystal axis parallel to ND) c) KAM Map (100 nm, 5°) d) non-martensite- martensite HAGB map, e) IQ map and f) SE SEM image of DER bands causing martensite fragmentation (arrow).Images were taken at a depth of 160 µm from surface.

3.4 Nanoindentation Analysis of DER

Nano-indentation, involving an indent matrix of 10 × 40 with 5 µm spacing in both directions covering an area from the contacting surface to a depth of 400 µm has been conducted on virgin and RCF tested 50CrMo4 bearings.. The maximum indentation penetration depth was maintained at 900 nm. Given that the 100Cr6 bearings in this study demonstrated developed stages of WEBs, it was difficult to isolate the influence of WEBs and DER separately, hence only the 50CrMo4 samples are tested in this section. The average hardness of the virgin sample is recorded to be 7.98 ± 0.2 GPa. Figure 15 shows the optical image of the indentation map and corresponding hardness change across the depth in reference to the virgin sample for the 50CrMo4 specimens run at different stress cycles to demonstrate the hardness changes associated with the evolution of the DER. Since the main purpose of the analysis is to investigate the hardness changes in the DER, locations were selected avoiding LAB interference. As the DER becomes more pronounced at early stages (from Figure 15a to Figure 15b), a hardness reduction can be observed in the highlighted region. However, at later stages, an increase in hardness (compared to virgin sample) is observed corresponding to the region that becomes 'brighter' or more resistant to etching at later stages (see the optical images of Figure 15c and d). The correlations between the higher hardness and higher etching resistance can be linked to the refinement of the microstructure evidenced through the EBSD analysis in this study. The heavier etched regions of the DER in Figure 15c and 15d beneath the bright layer is also associated with a reduced hardness due to the difference in grain sizes evidenced in Figure 8. Changes in the hardness is also

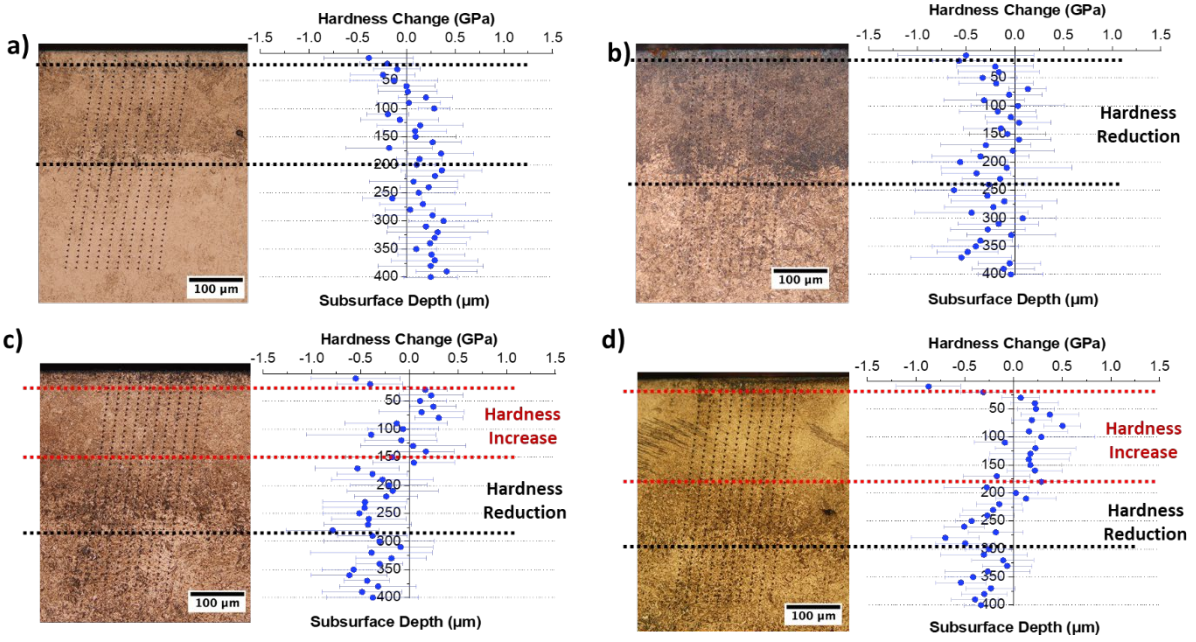

Figure 15: Optical images of indentation map and corresponding hardness changes across the subsurface depth between the virgin 50CrMo4 sample and samples tested for a) 158 million cycles b) 846 million cycles c) 2038 million cycles and d) 7668 million cycles.

observed outside the DER regions in Figure 15 which could be linked to potential competing mechanisms of initial work hardening and phase transformation in the overall microstructure [1, 11]. Nonetheless, a clear change in hardness profile is detected corresponding with the evolution stages of the DER.

4 Discussion

This study has shown that the initial stages of DER development appears as individual dark etching bands with a thickness varying between 30 and 100 nm and length of up to 7 µm. The characterisation of these bands has been challenging due to their small dimensions. The investigation in this study has revealed bright structures adjacent to dark etching bands (Figures 6-10) resembling the etching response of lenticular carbides in WEB [27]. Hence it is suspected to be some kind of carbide structure. As the dark etching bands are assumed to be ferritic [22, 16, 20, 36], the existence of carbide structures adjacent to these bands (best observed in Figure 10b) would suggest a carbon migration from the dark etching bands within the DER to their edges in a similar manner to the elongated ferrite grains and lenticular carbide formed in LABs [27]. This would contradict previous models based on a dislocation-assisted carbon migration from ferrite bands to pre-existing nano- sized tempered carbide [36]. Based on the observations obtained from this study that carbide-like structures formed adjacent to dark etching bands within DERs, it is thus suggested that the carbon migration links to the formation of new carbides rather than thickening pre-existing tempered carbides. However, the role of tempered carbides in the DER formation remains unclear. The fact that DER formation and development in the low carbon steel 50CrMo4 is much more pronounced than that in the high carbon 100Cr6 steel, which contains a large amount of primary spherical carbides while the low carbon steel contains none, indicates that primary carbides are not pre-requisite for DER formation. This agrees with a previous study reporting the distribution of primary carbides within the DER to be similar to its distribution in a virgin microstructure [22]. Nonetheless, further high-resolution examination of the carbides associated with DERs is needed to confirm the carbon migration patterns and carbide structures influencing it.

In the analysis conducted in this study, it is discovered that the dark etching bands, which appear as groups of parallel bands, show to orientate in four dominated angles in relation to the rolling direction: a) 10 - 30°, b) 65 - 85° and c) 135 - 170° . Out of the three groups of orientation, group a) is the most commonly observed orientation followed by group b), which happen to be aligned with LAB and HAB orientations respectively. This is also coupled with the observation that near the upper boundary of the DER, where WEBs develop and particularly HABs [10], the probability of both group a) and b) angles become similar whereas going towards the lower boundary of the DER, where only LABs develop [10, 27, 22], the orientation is dominated by group a) which

resembles that of LABs. This suggests that the orientations of the dark etching bands may be linked to preferential slip systems within the steel microstructure with some more activated than others. Texture analysis of LABs and HABs has been previously investigated to show elongated grains developing in these features have preferential slip systems of <111>{112} aligned at approximately 30° and 80° to the rolling direction respectively [22, 27, 37]. A texture analysis was attempted to investigate the dark etching bands but was inconclusive due to the difficulties encountered in capturing the extremely small dark etching bands within the DER. However, it remains unclear why the third orientation group (group c) does not correspond to the WEB orientations. It could be associated with the distribution density, where this group is the least observed in the DER statistically. Nonetheless, the statistical evidence shown in Figure 7 aligns with the orientation and position of LABs and HABs which suggests the stress or strain component controlling the orientation of the WEBs is influencing the material deformation early on from the DER stage.

The development of the dark etching bands in the DER corresponds with the fragmentation of the parent martensite microstructure (Figure 11) as the bands penetrate through martensite laths. At later stages, as the dark etching bands become denser, they appear as dark patches under LOM [22]. Within the dense patches of dark etching bands, a gradual grain refinement is observed (Figure 11-13). Based on the relatively high misorientation detected within these refined grains, they are likely a product of martensite fragmentation induced by plastic deformation. Equiaxed grains with low misorientation are detected within the DER patches as well with the dense dark etching bands (Figure 11c and Figure 14c), which are suggested as products of recrystallization. These equiaxed grains appear to nucleate at the high stress points arising from the refinement process due to the dense dark etching bands formation across martensite laths. Previous studies on alloys under cold rolling and compression tests have reported that deformation bands [38] and shear bands [39] are preferential sites for recrystallization nucleation due to greater dislocation density at bands intersections (evidenced in Figure 9). Shear bands subdivides the original martensite structure into finer grains, introducing more misorientation and stress points. Such a deformed structure could promote recrystallization in DER patches [40] also evidenced in Figure 11. This suggests that dark etching bands are a form of shear bands, which develop to cause refinement at intersection points of the dark etching bands of different orientations within the DER.

While early stage DERs consists of multiple dense dark etching bands at different distinct orientations, the bands become less pronounced during later stages due to formation of a refined microstructure (Figure 8 and Figure 12-13). Given that the dark etching bands are responsible for the dark etch response observed under LOM, this would explain why the region shows to have ‘brighter’ or more etch-resistant areas at later stages, due to breakdown of

the dark etching bands occurring alongside the refinement of the original parent microstructure which also leads to more resistance to etching and higher light reflectivity. A TEM investigation on adiabatic shear bands by Li et al [41]. has proposed a refinement mechanism of elongated ferrite grain structures, where under a high shear stress, the elongated grain (see Figure 16) containing clusters of entangled dislocations goes through partitioning and/or breaking down of the grain by entangled dislocation clusters and splitting and rotating of the grain respectively, leading to the formation of subgrains. The splitting may be enhanced as bands of different orientation intersect, leading to further grain refinement. A similar finding by Kang et al. [42] showed the DER to consist of fragmented areas where dynamic recrystallization also occurs. This refinement has been shown in this study to develop from the formation of dark etching bands intersecting martensite laths. A previous study has proposed that dark etching response occurs due to carbon flux from the matrix to adjacent carbides driven by Cottrell atmospheres migrating due to dislocation gliding [9]. However, this study has shown the specific dark etch response corresponds to individual dark etching bands. The structure of the individual dark etching bands is challenging to investigate given their size but the high stress points surrounding them suggests they are a form of shear bands induced by plastic deformation. Hence the dislocation re-arrangement within these individual shear bands (driven by the shear stress) would transport the carbon from within the band to its edge (causing martensite-ferrite phase transformation), leading to the formation and thickening of carbides. Growth of dark etching areas and softening has been reported by Kang et al. [42] for tests reaching 50 million cycles. However, long tests in this study of 7886 million cycles has clearly shown the dark etching response of the area diminishes at late-stages due to the removal of the dark etching bands due to continuous refinement while the small carbides remain.

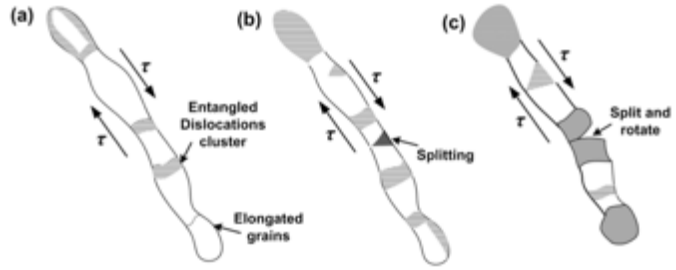

Figure 16: A schematic illustration of the grain refinement process (a)the elongated grain and entangled dislocation clusters at various sections; (b) grain refinement either through partitioning and breaking down the elongated subgrains by entangled dislocations clustering or through splitting and rotating the elongated subgrains into small grains; (c) subgrains formed [41].

The proposed refinement process in the DER is supported by the hardness increase evidence shown in Figure 15. While the hardness of DER reported in literature has been confusing, e.g. a reduction was reported in [9, 12] and an increase in [21, 8], the refinement process involved in DER development discovered in this study shows that the two competing mechanisms, i.e. softening due to ferrite formation and hardening due to carbon migration and

refinement of parent microstructure, provides the required answers. However, carbon redistribution has been reported to be minimal at micro-scale [22] or more observable at nano-scale and atomic scale [9, 42] thus its influence on DER development is likely to be modest when comparing the overall microstructure hardness. Kang et al. [42] showed hardness reduction proposed to be due to the reduction of carbon in the matrix, recrystallization and carbide thickening. However, it is interesting that results from this study show the opposite where a hardness increase is observed in the DER in the region that becomes brighter due to refinement. However, in Figure 15d, a relative reduction in hardness is observed corresponding the area that etches darker as the grains are coarser and some dark etching bands remain visible.

The brightened region in DER in Figure 15c and d also corresponds to the position of the earliest stage LAB detected in the 50CrMo4 samples which suggests a link between the DER brightening and the formation of LAB. From the earliest stages, shown in Figure 3, it can be seen that the DER formation corresponds with the material response to the orthogonal shear stress, similar to previous findings [9, 42]. However, the region transforms further and becoming brighter corresponds with the maximum von Mises stress at the latest stages. Therefore, it seems the formation of dark etching bands is linked to the orthogonal shear stress while the recrystallization of equiaxed grains at later stages corresponds with the von Mises stress. This is similar to the initiation and growth pattern of the LAB which has been linked to the von Mises stress [10, 33, 27]. This provides evidence of a link between the two features which is further explored in the following section for the proposed formation mechanism of the DER and its transition to LAB.

5. Formation Mechanisms

The first stage of microstructural alterations is the formation of the DER that initiate when dark etching bands develop in parent microstructure (see Figure 17b). These bands appear to have smooth etch-resistant structures at their edges that are similar to lenticular carbides found in WEBs at larger scale. This suggests that similar to LABs, carbide-like structures develop at the edge of these dark etching bands within DER which could be related to dislocation rearrangement under applied cyclic stress within the bands (see Figure 17b). These bands grow in density across the maximum shear stress region in patches at distinct orientations to the rolling direction (Figure 17c and d) giving the dark etch response under LOM. As the dark etching bands become denser, a refinement

process intensifies within DER through fragmentation of martensite laths (see Figure 17c), which is more

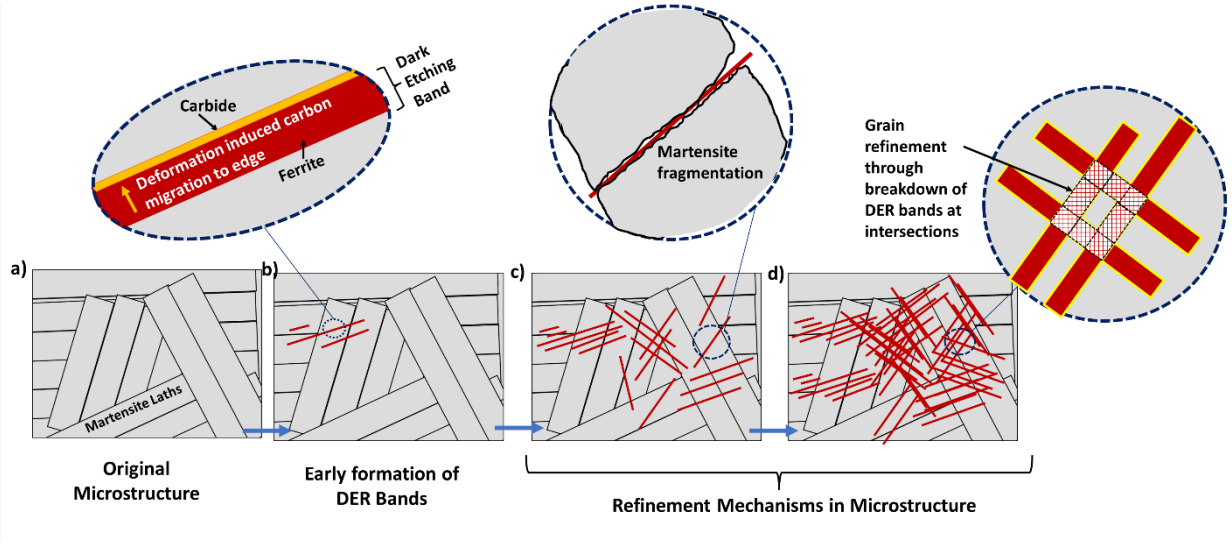

Figure 17: Schematic of microstructural alteration stages in DER showing a) original microstructure consisting of martensite laths. b) Development of DER bands in parent microstructure which consist of carbide-like structure at the edge likely due to carbon migration across the DER band. c) More DER bands develop at different orientations which result in the fragmentation of martensite laths leading to refinement of the region. d) DER bands become dense leading to dark patches where the DER bands eventually breakdown due to intersections between different DER bands at different orientations.

pronounced in the maximum shear stress region. At late-stages, the dark etching bands are seen to become less frequently observed while more and more equiaxed/fine grains are formed in the region (resulting in higher hardness and brighter appearance when etched). This is suggested also due to breakdown of dark etching bands at band intersections (Figure 17d).

The DER formation mechanism can be summarized initially as the development of dark etching bands in the martensitic matrix (Figure 17c and d) which is similar in nature to deformation bands commonly observed in deformed materials [38] [39] [41]. Hence these dark etching bands or deformation bands, are likely induced via plastic deformation induced dislocation re-arrangement driving the transportation of carbon during the martensite-ferrite phase transformation and potential carbide formation at the edge of these bands. EBSD evidence in this study has shown that as these dark etching bands become denser and cause the eventual refinement of the microstructure, this results in a build-up of stress points across the DER area with high mis-orientation. These stress points become initiation sites for recrystallization of low misorientation equiaxed grains (schematically shown in Figure 18b). The formation of these low misorientation equiaxed grains has also been observed at the intersection of dark etching bands (shown schematically in Figure 18c) and observed in Figure 9 due to enhanced dislocation density at these locations [38] [39].

The formation of both dark etching bands and equiaxed grains is considered to be martensite-ferrite phase transformations although they clearly have different properties and formation mechanisms. The dark etching

bands develop initially at distinctive orientations to the rolling direction (see Figure 6 and 7) and grow in density across the subsurface area with the highest orthogonal shear stress with increasing cyclic loading. Hence it is proposed that the carbon transportation in this stage is mainly governed by the stress induced dislocation rearrangement within these small bands. The equiaxed ferrite grains due to recrystallization, identified by its low misorientation, originates at high stress point caused by the bands and refinement. At this stage, the transportation of carbon is more likely governed by temperature. However, it should be noted that the influence of temperature and plastic deformation (due to shear stress) cannot be negated in both cases as temperature is known to influence the mobility of dislocation gliding and diffusion of free carbon. The influence of both temperature and stress on DER formation is well documented [9, 19] . However, it is proposed that the influence of each parameter varies at the different stages of DER development.

The next stage of RCF-induced microstructural transformation is the formation of WEB (LAB initially followed by HAB) which has been reported previously to initiate as only a small band of equiaxed ferrite grains [27] similar to the equiaxed grains reported in this study. A link can therefore be established between DER and LAB where the energy build-up in the DER patches due to the formation of dense dark etching bands and martensite fragmentation nucleate the equiaxed ferrite grains that grows into the early-stage LAB reported. However, why the equiaxed ferrite grains grow as bands at the orientations of ~30° to the rolling direction could be explained by the DER distribution. The most common orientation of the dark etching bands (10 – 30°) in this study is similar to the orientation of LAB (20 - 35°), hence given that recrystallization occurs in regions with the highest dislocation densities/ energy build-up, the recrystallization process developing the equiaxed ferrite grains could follow the distribution of the pre-existing dark etching bands induced by plastic deformation, leading to the transition from DER to LAB in the microstructure. Further microstructural transformation due to RCF after DER, i.e. formation of LAB and HAB, has been detailed in [27]. Hence the orientation of the LAB could be correlated with the density of the dark etching bands which are initiation sites for recrystallization as discussed previously. This explains why the equiaxed grains of the LAB (first stage of LAB development as stated in [27]), follow this orientation. The equiaxed grains of both LAB and HAB has been reported to transition to elongated grains through a grain rotation/coalescence mechanism [27] leading to texturing of the elongated grains. A preferential slip system of <111>{112} has been found orientated at 30° and 80° in LAB and HAB respectively to explain the deformation orientation [22, 27, 37] with respect to the rolling direction. It remains unclear whether a similar texture exists in the dark etching bands of the DER. The orientation of the dark etching bands is also seen to vary across the depth like WEBs (LABs and HABs [10, 7, 1]). It has also been discussed in [27] that HAB forms due

to the dissolving of unstable lenticular carbides of the LAB. Similar to the orientation of the dark etching bands in this study, this would suggest the deformation induced in the 65-85° orientation is most effective in breaking down these unstable carbides during the LAB/HAB transition. However, it remains unclear why the third orientation group found in this study (135-170°) does not correlate with developing WEB features. It is likely to be correlated to their relatively lower density compared to the other orientation groups coupled with the orientation most influential in breaking down lenticular carbides in LABs. Nonetheless, the future work in this field should focus on investigating modelling stress/strain components most likely to contribute to these distinct orientation groups originating directly form the parent matrix in the form of DER which appear to govern the following microstructural alterations steps in the form of LAB and HAB.

While the proposed unified formation mechanism explains the sequential development of DER,LAB and HAB which has been experimentally observed in multiple studies [10, 33, 6, 19, 11, 17, 24, 8, 7], there have been studies reporting WEB formation in the absence of the DER [43, 44] in low tempered steels with a hardness < 720 HV. Based on the DER evolution mechanism observed in this study where the DER loses its characteristic etching response (becomes brighter) at late stages due to the breakdown of the dark etching bands, it is likely that the DER may have been 'removed' at that stage. However, another explanation is that these soft steels (due to low tempering) are heavily deformed from earlier stage, leading to a build-up of stress points earlier in the bearing life which directly initiate the LAB stage without the need of DER. The gradual build-up of stress points in the microstructure due to DER might be necessary for higher tempered steels (typical bearing tempering conditions) whereas softer steels can experience this deformation earlier without the need for DER to develop. Further microstructural analysis into these soft steels at early stages would be needed to further investigate this.

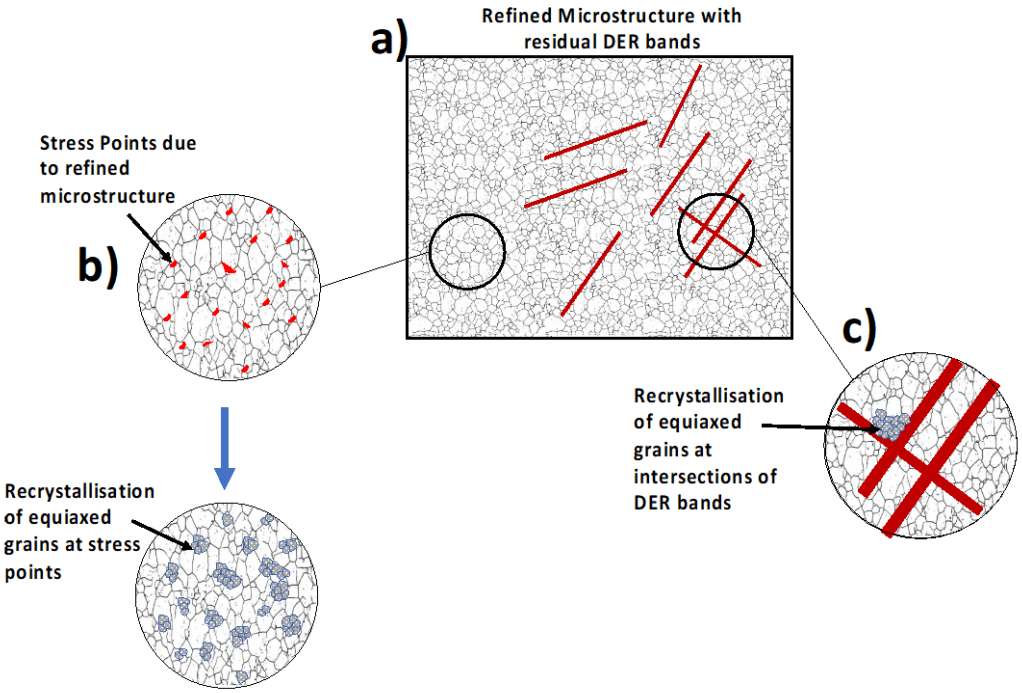

Figure 18: a) Schematic of late stage DER consisting of refined microstructure resulting from the refinement mechanisms in Figure 17 and remaining DER bands still intact. b) Stress points due to refined microstructure due to martensite fragmentation becoming nucleation sites for recrystallization and equiaxed ferrite grain formation. c) Recrystallization of equiaxed ferrite grains nucleating at intersections of dark etching bands.

6. Conclusions

The investigation of DER formation mechanisms has initially been conducted on the hypoeutectoid steel 50CrMo4 bearings, where its development stages are captured through detailed analysis using a combination of BSE and SE SEM imaging, EBSD analysis and nanoindentation. Comparing to formation in 100Cr6, has provided firm evidence on its formation and evolution mechanism. It has also been linked to the formation of LABs, together with findings from a previous study by the authors [27], a unified formation mechanism for all classical RCF-induced transformations (DER, LAB and HAB) has been established. The conclusions of the current study on DER are summarized below.

- Initial stage of DER formation consists of the development of thin dark etching bands that grow in density as patches of different orientations. The heavy etching of these bands gives the dark etch response of the DER under LOM due to a diffuse reflection of the light on the resulting rough topography. The dark etching bands, which grows in the region of highest orthogonal shear stress, contributes to martensite fragmentation and refinement as they become denser. The refined microstructure is found to have an increased hardness.

- The dark etching bands in DER are shown to have orientations at three dominant angles inclined to the rolling direction at 10 - 30°, 65 - 85°, and 135 - 170°. The most frequent orientation group observed is 10 - 30° followed by 65 - 85°, which happened to be coincided with the orientations of LAB and HAB respectively.
- Bright structures at dark etching band edges are observed in SEM which show a similar etching response to the lenticular carbides in the WEB. Hence these are proposed to be newly formed carbides forming in DER due to carbon migration from the bands.
- At late-stages of DER development, dark etching bands become less pronounced due to their breakdown and refinement of the overall microstructure, leading to a brighter appearance under LOM due to a more directed reflection of light. The breakdown is caused by the intersection of multiple dark etching bands at various orientations. The developed microstructure consists of fine grains from martensite fragmentation and equiaxed grains with low misorientation as a product of recrystallization. High stress points formed in dense dark etching bands areas, due to martensite fragmentation and intersecting points of different dark etching bands, act as nucleation sites for equiaxed ferrite grains with low misorientations.
- The formation of the low misorientation equiaxed ferrite grains in the DER marks the onset of LAB initiation which later grows as bands at orientations similar to that of the most common orientation group of the dark etching bands (10-30°).

The gradual development of DERs has been successfully recorded in this study to demonstrate the stages in which it initiates and evolves during bearing operation. It is concluded that the RCF-induced transformation of the parent microstructure to DER initiates from plastic deformation of the microstructure along preferential planes leading to the formation of ferritic dark etching bands and carbon diffusion across the band to form carbides. These bands result in the refinement of the microstructure and contribute to high stress points distributed across the DER area which later become nucleation sites for the recrystallization of equiaxed ferrite grains. The newly formed equiaxed ferrite grains later grow as large bands known as LABs and later transform to HABs which also develops in a similar manner to the DER [27]. Hence it can be concluded that the sequential formation of all three microstructural transformations (DER, LABs and HABs) are a direct result of a repetitive cycle of energy build-up and release in the microstructure due to the RCF-induced cyclic stresses driven by plastic deformation and carbon diffusion.

7. Acknowledgement

This research has been co-funded by ESPRC (EP/N509747/1) and Schaeffler Technologies AG & Co. KG, Schweinfurt, Germany.

References

[1] M. El Laithy, L. Wang, T. J. Harvey, B. Vierneusel, M. Correns and T. Blass, "Further understanding of rolling contact fatigue in rolling element bearings-a review," *Tribology International,* p. 105849, 2019.

[2] V. Šmeļova, A. Schwedt, L. Wang, W. Holweger and J. Mayer, "Microstructural changes in White Etching Cracks (WECs) and their relationship with those in Dark Etching Region (DER) and White Etching Bands (WEBs) due to Rolling Contact Fatigue (RCF)," *International Journal of Fatigue,* vol. 100, pp. 148-158, 2017.

[3] M. Evans, "An updated review: white etching cracks (WECs) and axial cracks in wind turbine gearbox bearings," *Materials Science and Technology,* vol. 32, pp. 1133-1169, 2016.

[4] M. Evans, L. Wang and R. Wood, "Formation mechanisms of white etching cracks and white etching area under rolling contact fatigue," *Proceedings of the Institution of Mechanical Engineers, Part J: Journal of Engineering Tribology,* 2014.

[5] A. B. Jones, "Metallographic Observations of Ball Bearing Fatigue Phenomenom," in *Symposium on testing of bearings*, Philadelphia, ASTM International, 1947.

[6] J. J. Bush, W. L. Grube and G. H. Robinson, "Microstructural and Residual Stress Changes in Hardened Steel due to Rolling Contact," *Trans. ASM,* vol. 54, pp. 390-412, 1961.

[7] A. Warhadpande, F. Sadeghi and R. D. Evans, "Microstructural alterations in bearing steels under rolling contact fatigue Part 1—Historical overview," *Tribology Transactions,* vol. 56, pp. 349-358, 2013.

[8] S. Echeverii Restrepo, S. Ooi, P. Yan, P. Andric, R. Vegter and J. Lai, "Dark etching regions under rolling contact fatigue: a review," *Materials Science and Technology,* vol. 37, no. 4, pp. 347-376, 2021.

[9] H. Fu, W. Song, E. I. Galindo-Nava and P. E. J. Rivera-Díaz-del-Castillo, "Strain-induced martensite decay in bearing steels under rolling contact fatigue: modelling and atomic-scale characterisation," *Acta Materialia,* vol. 139, pp. 163-173, 2017.

[10] M. El Laithy, L. Wang, T. Harvey and B. Vierneusel, " Re-investigation of dark etching regions and white etching bands in SAE5 2100 bearing steel due to rolling contact fatigue," *International Journal of Fatigue,* vol. 136, p. 105591, 2020.

[11] A.Voskamp, "Material Response to rolling contact loading," *J Tribol,* vol. 107, pp. 359-364, 1985.

[12] H. P. C. O. Swahn, P. C. Becker and O. Vingsbo, "Martensite decay during rolling contact fatigue

in ball bearings," *Metallurgical transactions A,* vol. 7, pp. 1099-1110, 1976.

[13] N. H. Forster, L. Rosado, W. P. Ogden and H. K. Trivedi, "Rolling contact fatigue life and spall propagation characteristics of AISI M50, M50 NiL, and AISI 52100, Part III: metallurgical examination," *Tribology Transactions,* vol. 53, pp. 52-59, 2009.

[14] G. Vasilca and V. Raszillier, "A study of dark etching area (D.E.A.) type structure modification of material and hertzian contact area induced by ball bearing type motion," *Wear,* vol. 19, no. 1, pp. 1-15, 1972.

[15] R. Österlund and O. Vingsbo, "Phase changes in fatigued ball bearings," *Metallurgical Transactions A,* vol. 11, pp. 701-707, 1980.

[16] I. A. Polonsky and L. M. Keer, "On white etching band formation in rolling bearings," *Journal of the Mechanics and Physics of Solids,* vol. 43, pp. 637-669, 1995.

[17] J. A. Martin, S. F. Borgese and A. D. Eberhardt, "Microstructural alterations of rolling—bearing steel undergoing cyclic stressing," *Journal of Basic Engineering,* vol. 88, pp. 555-565, 1966.

[18] N. G. Popinceanu, E. Diaconescu and S. Cretu, "Critical stresses in rolling contact fatigue," *Wear,* vol. 71, pp. 265-282, 1981.

[19] M. Abdullah, Z. Khan and W. Kruhoeffer, "Evaluation of Dark Etching Regions for Standard Bearing Steel under Accelerated Rolling Contact Fatigue," *Tribology International,* vol. 152, p. 106579, 2020.

[20] A. King and J. O'Brien, "Microstructural alterations in rolling contact fatigue," in *Advances in Electron Metallography*, ASTM International , 1966.

[21] H. Muro and N. Tsushima, "Microstructural, microhardness and residual stress changes due to rolling contact," *Wear,* vol. 15, pp. 309-330, 1970.

[22] V. Šmeļova, A. Schwedt, L. Wang, W. Holweger and J. Mayer, "Electron microscopy investigations of microstructural alterations due to classical Rolling Contact Fatigue (RCF) in martensitic AISI 52100 bearing steel," *International Journal of Fatigue,* vol. 98, pp. 142-154, 2017.

[23] J.-H. Kang, B. Hosseinkhani and P. E. J. Rivera-Díaz-del-Castillo, "Rolling contact fatigue in bearings: multiscale overview," *Materials Science and Technology,* vol. 28, pp. 44-49, 2012.

[24] k. Sugino, K. Miyamoto, M. Nagumo and K. Aoki, "Structural alterations of bearing steels under rolling contact fatigue," *Transactions of the Iron and Steel Institute of Japan,* vol. 10, no. 2, p. 98, 1970.

[25] A. Voskamp and E. Mittemeijer, "Crystallographic preferred orientation induced by cyclic rolling contact loading," *Metallurgical and Materials transactions A,* vol. 27, no. 11, pp. 3445-3465, 1996.

[26] J. Kang, "Mechanisms of microstructural damage during rolling contact fatigue of bearing steels," in *PhD Thesis*, 2014.

[27] M. El Laithy, L. Wang, T. Harvey, A. Schwedt, B. Vierneusel and J. Mayer, "White etching bands formation mechanisms due to rolling contact fatigue," *Acta Materialia,* p. 117932, 2022.

[28] D. Markus and T. Werner, "Influence of Sulfur Inclusion Content on Rolling contact Fatigue Life," *Bearing Steel Technology Advaned Steel Technology Rolling Bearings,* vol. 10, pp. 83-99, 2014.

[29] T. Furuhara, H. Kawata, S. Morito and T. Maki, "Crystallography of Upper Bainite in Fe–Ni–C Alloys," *Materials Science and Engineering: A,* vol. 431, pp. 228-236, 2006.

[30] H. Kitahara, R. Ueji, N. Tsuji and Y. Minamino, "Crystallographic Analysis of Plate Martensite in Fe–28.5 at.% Ni by Fe-SEM/EBSD," *Materials Characterization,* vol. 54, pp. 378-386, 2005.

[31] A. Greninger and A. Troiano, "Orientation Habit of Martensite," *Nature,* vol. 141, p. 38, 1938.

[32] Y. He, "Grain-Scale Characterization of Fcc/Bcc Correspondence Relations and Variant Selection," McGill University, Montreal, 2005.

[33] M. El Laithy, L. Wang, T. Harvey and B. Vierneusel, "Semi-empirical model for predicting LAB and HAB formation in Bearing Steels," *International Journal of Fatigue,* p. 106230, 2021.

[34] H. Fu, E. I. Galindo-Nava and P. E. J. Rivera-Díaz-del-Castillo, "Modelling and characterisation of stress-induced carbide precipitation in bearing steels under rolling contact fatigue," *Acta Materialia,* vol. 128, pp. 176-187, 2017.

[35] J. Kang and P. Rivera-Diaz-del-Castillo, "Carbide Dissolution in bearing steels," *Computational Materials Science,* vol. 67, pp. 364-372, 2013.

[36] H. Fu and P. E. J. Rivera-Díaz-del-Castillo, "A unified theory for microstructural alterations in bearing steels under rolling contact fatigue," *Acta Materialia,* vol. 155, pp. 43-55, 2018.

[37] K. Kanetani and K. Ushioda, "Mechanism of white band (WB) formation due to rolling contact fatigue in carburized SAE4320 steel," *MATERIALS TRANSACTIONS,* vol. 61, no. 9, pp. 1750-1759, 2020.

[38] Q. Luan, J. Wang, Y. Huang, D. Balint and J. Jiang, "How would the deformation bands affect recrystallization in pure aluminium?," *Materials & Design,* vol. 209, p. 109960, 2021.

[39] Y. Tian, O. Gorbatov, A. Borgenstam, A. Ruban and P. Hedstrom, "Deformation microstructure and deformation-induced martensite in austenitic Fe-Cr-Ni alloys depending on stacking fault energy," *Metallurgical and materials transactions A,* vol. 48, 2017.

[40] K. K. Alaneme and E. A. Okotete, "Recrystallization mechanisms and microstructure development in emerging metallic materials: A review," *Journal of Science: Advanced Materials and Devices,* vol. 4, pp. 19-33, 2019.

[41] S.-X. Li, P.-C. Zhao, Y.-N. He and S.-R. Yu, "Microstructural evolution associated with shear location of AISI 52100 under high strain rate loading," *Materials Science and Engineering: A,* vol. 662, pp. 46-53, 2016.

[42] J.-H. Kang, J. Kim, J.-Y. Kang, S.-W. Kwon, M.-W. Kang and S. H. Hong, "Multiscale study on the dark-etching region due to rolling contact fatigue of 0.57C-bearing steel," *Acta Materialia,* vol. 226, p. 117666, 2022.

[43] H. Fu and P. E. J. Rivera-Díaz-del-Castillo, "Evolution of White Etching Bands in 100Cr6 Bearing Steel under Rolling Contact-Fatigue," *Metals,* vol. 9, p. 491, 2019.

[44] T. Lund, "STRUCTURAL ALTERATIONS IN FATIGUE-TESTED BALL- BEARING STEEL," *Jernkontorets Ann,* vol. 153, pp. 337-343, 1969.

[45] O. Zwirlein and H. Schlicht, "Rolling contact fatigue mechanisms—accelerated testing versus field performance," in *Rolling contact fatigue testing of bearing steels*, ASTM International, 1982.

[46] H. Fu, "Microstructural alterations in bearing steels under rolling contact fatigue," 2017.

[47] A. T. W. Barrow, J.-H. Kang and P. E. J. Rivera-Díaz-del-Castillo, "The ε→ η→ θ transition in 100Cr6 and its effect on mechanical properties," *Acta materialia,* vol. 60, pp. 2805-2815, 2012.